(12) **LEVEL** *II*

DNA 5261F

AD A090533

PHOTON SOURCE SGEMP
SPECTRUM EVALUATIONS

A. J. Woods
E. P. Wenaas
JAYCOR
1401 Camino Del Mar
Del Mar, California 92014

24 April 1978

Final Report for Period 18 July 1977—18 February 1978

CONTRACT No. DNA 001-77-C-0277

Prepared for

Director

DEFENSE NUCLEAR AGENCY

Washington, D. C. 20305

80 10 10 08

UNCLASSIFIED

REPORT DOCUMENTATION PAGE	READ INSTRUCTIONS BEFORE COMPLETING FORM

1. REPORT NUMBER	2 GOVT ACCESSION NO	3 RECIPIENT'S CATALOG NUMBER
DNA 5261F	AD-A090533	

4. TITLE (and Subtitle)	5. TYPE OF REPORT & PERIOD COVERED
PHOTON SOURCE SGEMP SPECTRUM EVALUATIONS	Final Report for Period 18 Jul 77—18 Feb 78
	6 PERFORMING ORG REPORT NUMBER

7. AUTHOR(s)	8. CONTRACT OR GRANT NUMBER(s)
A. J. Woods and E. P. Wenaas	DNA 001-77-C-0277

9 PERFORMING ORGANIZATION NAME AND ADDRESS	10 PROGRAM ELEMENT PROJECT TASK AREA & WORK UNIT NUMBERS
JAYCOR 1401 Camino Del Mar Del Mar, California 92014	Subtask G37LAXYX960-04

11. CONTROLLING OFFICE NAME AND ADDRESS	12. REPORT DATE
Director Defense Nuclear Agency Washington, D.C. 20305	24 April 1978
	13 NUMBER OF PAGES 84

14 MONITORING AGENCY NAME & ADDRESS(if different from Controlling Office)	15 SECURITY CLASS (of this report)
	UNCLASSIFIED
	15a DECLASSIFICATION DOWNGRADING SCHEDULE

16 DISTRIBUTION STATEMENT (of this Report)

Approved for public release; distribution unlimited.

17 DISTRIBUTION STATEMENT (of the abstract entered in Block 20, if different from Report)

18 SUPPLEMENTARY NOTES

This work sponsored by the Defense Nuclear Agency under RDT&E RMSS Code B323077462 G37LAXYX96004 H2590D.

19 KEY WORDS (Continue on reverse side if necessary and identify by block number)

SGEMP	TREE
X-ray Photon Source	Cable Excitation
Photo-Compton Emission	
Dose	

20 ABSTRACT (Continue on reverse side if necessary and identify by block number)

Methods of evaluating photon spectra for SGEMP effects are discussed. A set of evaluation parameters is selected which may be readily computed for arbitrary photon spectra in the range 1 to 1000 keV. Representative satellite positions and materials are described, and the parameters are tabulated for certain classes of spectra. Algorithms are provided for relating the tabulated values to arbitrary photon spectra. Both linear and nonlinear responses are treated and sample computations performed. Descriptions and user

DD FORM 1473 EDITION OF 1 NOV 65 IS OBSOLETE

UNCLASSIFIED

20. ABSTRACT (Continued)

instructions for programmable calculator codes to compute the parameters for arbitrary photon spectra are given.

TABLE OF CONTENTS

LIST OF TABLES

LIST OF ILLUSTRATIONS

1. INTRODUCTION

The purpose of this effort is to provide quantitative information to aid in evaluating the effects of x-ray spectral variations on the SGEMP response of satellite systems. The problem is approached by defining a number of excitation parameters such as electron yield and velocity, dose, dipole moment, etc., which are the driving functions for the various SGEMP effects. The driving functions are evaluated at various locations in a representative satellite structure ranging from the external surface through various structural elements to heavily shielded equipment boxes.

The excitation parameters chosen are basically linear and can, therefore, be computed as a function of incident x-ray energy. Coefficients are computed which relate the various excitation parameters to incident x rays such that the excitation parameters can be obtained for an arbitrary spectrum. The effects of various x-ray spectra can be evaluated by comparing the excitation parameters produced by candidate sources with those produced by blackbodies or weapon spectra of interest. All excitation parameters are computed for blackbody spectra ranging from 1 to 15 keV.

While most of the excitation parameters chosen are linear with x-ray fluence, it should be noted that many of the x-ray responses are nonlinear. It is of some interest to evaluate certain "response" parameters to determine the range in which responses become nonlinear. However, the nonlinear response parameters are not the most suitable for evaluating x-ray spectra because the effects tend to become less sensitive to spectral variations in the nonlinear regime (Ref. 1). Because the responses are more sensitive to spectral variations in the linear regime, and because linear responses occur at numerous locations on spacecraft over virtually the entire range of interest, the linear response parameters give a better indication of the maximum response variations caused by spectral variations.

The nonlinear responses can be somewhat artificially divided into two categories of problems — the internal response of internal cavities and the external response of convex objects where a certain fraction of the electrons can escape from the object. Spectral effects on the nonlinear internal cavity response are evaluated with a quasistatic 1-D solution with emission

from one face of a diode. The potential, transmitted current, and dipole moment are used as response parameters. The external response evaluation in the nonlinear regime is not treated here.

Because of the potentially tedious calculations required to evaluate an arbitrary spectrum and compare excitation parameters with those of blackbody spectra or weapons, a set of magnetic cards for the TI-59 calculator has been prepared. These cards are available and can readily be used to compute each of the parameters considered in this effort.

2. SPECTRUM EVALUATION PARAMETERS

There exists a myriad of parameters that could be chosen to evaluate SGEMP response sensitivities to x-ray spectrum variations. One approach consists of identifying all important known effects and defining responses (e.g., fields, currents, potentials, etc.) for representative configurations or geometries of possible interest. Such an approach tends to depend upon the configuration or model chosen and might also result in an excessive list of evaluation parameters.

A second approach is to define the quantities responsible for producing each of the known effects. Presumably, if each of the driving functions or excitation parameters is specified, the responses resulting from these excitation sources will also be uniquely specified. Implicit in this treatment is the assumption that an x-ray spectrum which produces excitation terms comparable to a second spectrum will also produce similar SGEMP responses. This approach precludes the need for defining complex geometries and performing complicated time-dependent calculations, and was chosen for this effort.

A distinction between excitation and response terms may be helpful at this point. Parameters which are linear with fluence and independent of x-ray pulse time history are termed "excitation" parameters. Parameters that become nonlinear as space-charge-limiting becomes appreciable, and are dependent on pulse time history, are called "response" parameters. Furthermore, source terms are dependent only upon attenuation and emission materials, whereas response terms are also dependent on geometry.

Primary emphasis in this effort is on defining a pertinent set of excitation parameters and evaluating them at suitable points on a representative spacecraft. A limited set of response parameters is considered to obtain a first-order characterization of spectral response to space-charge-limiting. Solutions are kept as general as possible, and lend themselves to analytic treatment.

Variations in x-ray time history are not specifically considered in this exercise. Effects due to different pulse widths of spectra can be readily estimated in the linear regime. Evaluations of simultaneous spectral

and temporal variations in the nonlinear regime are very complex and beyond the scope of this simple treatment.

The parameters chosen for evaluating spectra are summarized in Table 1. The list is not exhausive but is representative of the terms thought to be important in producing x-ray responses. The parameters can be conceptually divided into four categories: the electron yield which is the basic x-ray interaction with the materials; the dipole moment in a dielectric which is descriptive of the charge deposition profile; the energy deposition in dielectrics and semiconductors; and finally, several quantities such as average velocity and energy and dipole moment which are descriptive of the location and motion of charge in a vacuum.

Table 1. Parameters Employed in Comparing SGEMP Effects
of Different Photon Spectra

Electron Yield
     Primary yield
     Forward-to-reverse ratio
     High-to-low-Z ratio
Dielectric Charge Profile
     Dipole moment
Dose
     Bulk dose
     Interface dose
     Dose ratio (Au/Si)
Vacuum Charge Profile
     Mean electron velocity
     Average electron energy
     Diode potential
     Diode current
     Dipole moment

In terms of our definitions of excitation and response terms, we may categorize electron yield, dose, mean velocity and energy, and dielectric dipole moment as excitation terms. These quantities are not dependent on

flux rates, and are linear with fluence over the ranges of interest here. Diode potential, current, and dipole moment are classified as response terms. These require a specification of photon source flux and some minimal system geometry, and also may become nonlinear with fluence.

Four basic categories of x-ray response are being described by the parameters of Table 1. They are the external SGEMP response, internal cavity SGEMP response, shielded cable excitation, and TREE effects caused by energy deposition in electronics, as indicated in Table 2. The electron yield is important in every category in that it provides the basic coupling of photons into the system. Primary electron yield, as defined here, is the total number of electrons produced by an irradiated surface in the energy range above 100 eV (generally speaking). This yield is distinguished from secondary-electron yield (electrons of energy 100 eV and below) because analytic multiple-scattering cross sections are considered to be inaccurate below 1 keV (Ref. 2). Recent analytical work in the regime below 1 keV (Ref. 3) has not been incorporated here.

The external response in the linear regime is determined by the primary-electron yield in the reverse direction and by the average electron velocity. Under certain circumstances, forward-directed emission may be important also. Generally speaking, electron emission will occur from low-Z materials on the outside. Stored charge release of abundant low-energy electrons may also be an important SGEMP driver in the low-fluence regime. This secondary-electron yield has been shown to be proportional to interface dose (Ref. 4). The spectrum energy becomes important in the nonlinear regime, but the response in this regime is less sensitive to spectrum than in the linear regime and has not been treated.

The internal cavity response is highly dependent on electron yield ratios as well as on electron velocity. Cavities may be large (~ 2 m) with emission from either low-Z or high-Z materials. The net forward-to-backward emission ratio may be important in determining net current in cavities. The larger cavities may produce considerable space-charge-limiting at the higher fluence levels, and the average energy, diode potential and current, and dipole moment may be used to characterize the response (Ref. 5). Small cavities such as equipment boxes may contain higher-Z materials in sizeable proportions. High-to-low-Z electron emission ratios may be important in these cases.

11

Table 2. Summary of Parameters Describing
Each SGEMP Regime Treated Here

External Response

    Linear regime

        Electron yield

        Average velocity

        Interface dose

Internal Cavity Response

    Large cavities, linear regime

        Electron yield from low-Z materials

        Forward-to-reverse ratio

        Average velocity

        Interface dose

    Large cavities, nonlinear regime

        Diode potential, current

        Dipole moment

        Average energy

    Small cavities

        High-to-low-Z emission ratio

Cable Excitation

    Electron yield

    Dipole moment

    Dose

Energy Deposition in Electronics

    Bulk dose

    Interface dose

    Dose ratio (Au/Si)

The excitation of shielded cables by direct x-ray penetration is generally proportional to electron yield from cable shields for cables with large gaps, and proportional to the electron dipole moment resulting from penetration of electrons emitted from shielding material into the dielectrics for cables without gaps (Refs. 6,7,8). At the higher fluence levels, dielectric relaxation times may become comparable to response times of interest. These have been shown to depend upon dose and dose rate (Ref. 9).

Transient radiation effects in electronics (TREE) are dependent upon energy deposition due to photo-Compton electrons. The process is important both in the bulk (greater than an electron range from the surface) and at material interfaces. In the latter case, dissimilar materials can greatly affect energy deposition within an electron range of the interface (Ref. 10). This effect is represented well to first order by the ratio of the bulk dose in each material.

SGEMP parameters considered in this exercise but not directly employed in the spectral sensitivity studies are listed in Table 3. Certain of these quantities are not strong functions of photon or electron energy over the range of 1 to 1000 keV. For example, electron backscatter yield is a weak function of energy spectrum in this range (Ref. 11). Other quantities of interest may be well represented by a different parameter type as far as spectral sensitivity is concerned. Interface dose enhancement due to dissimilar materials falls into this category. The energy sensitivity of the interface-to-bulk dose ratio in a medium behaves similarly to the bulk dose ratio of the two mediums. Therefore, only the latter ratio has been included in the list. Secondary-electron yield has been shown to be proportional to surface dose [energy deposition with an electron range of the surface (Ref. 4)], and so has not been computed separately.

Table 3. Potentially Interesting Spectrum Evaluation Parameters
Not Treated Here Due Either to Weak Energy Dependence or
to Similar Sensitivity to These Quantities Listed in Table 1

Secondary-electron emission efficiency

Electron backscatter yield

Interface dose enhancement due to dissimilar materials

Electron angular distribution

---

3. SATELLITE LOCATIONS

Representative satellite materials and thicknesses have been chosen with assistance from TRW (Ref. 12), as shown in Table 4. The intervening materials are listed as well as the energy at which the photon attenuation is 1/e. Also indicated is the blackbody temperature for which the attenuation is 1/e. The locations have been chosen to range from the very thinnest (thermal blanket) to the very thickest (heavily shielded box), with a good sample of intervening thicknesses.

The materials on the external surface of the satellite tend to be low-Z such as quartz coverglass, fiberglass, and aluminum. Large internal cavity walls are also characterized by low-Z materials, although a significant amount of lead-tin solder is found on solar cells. The Faraday cage, thermal blanket, and solar cell models represent these types of wall materials. The thin mylar or thinnest Faraday cage (3 mils aluminum) is apt to produce the largest internal cavity response due to maximum electron emission. The thicker Faraday cage model and solar cell give a measure of the hardness of a spectrum required to penetrate thick wall materials.

A minimum-thickness equipment box wall (20 mils aluminum) is also modeled to produce the worst-case response driver in regions where vulnerable electronics are found. Various emission and dose ratios are obtained for this minimal attenuation. Addition of 10 mils Kovar represents a typical attenuation through the semiconductor case into the interior, and maximum spectrum attenuation is represented by the heavily shielded box model.

Minimum photon attenuations into cable interiors are represented by a shield model consisting of 3 mils copper; 20 mils copper is used to represent penetration by photons to a cable deep in the interior of a cable bundle.

Table 4. Satellite Locations

Satellite Location	Intervening Material	Energy [e-fold attenuation] (keV)	Blackbody Temperature [e-fold attenuation] (keV)
Surface	-	-	-
Thermal blanket	10 mils mylar	5	1-2
Faraday cage	3 mils aluminum (minimum)	8	2
	20 mils aluminum (maximum)	15	4
Solar cell	5 mils quartz 10 mils silicon 1 mil lead-tin solder 5 mils fiberglass 2 mils aluminum 5 mils fiberglass	22	7
Cable shield	3 mils copper (min. shield thickness)	28	8
	20 mils copper (behind bundle)	53	15
Box wall	20 mils aluminum (minimum)	15	4
Box & semi-conductor device housing	20 mils aluminum 10 mils Kovar	40	11
Heavily shielded box	20 mils aluminum 10 mils Kovar 12 mils tantalum	135	~35

4. EXCITATION PARAMETER CALCULATIONS

Satellite excitation parameters have been evaluated for selected sat-
ellite positions and materials. Unit fluence is assumed to be incident for
all configurations. Results are valid at all fluence levels, including the
nonlinear response regime. A modified version of the QUICKE2 electron emis-
sion code was used in the computations (Ref. 13).

The results presented here are questionable in the very low energy
limit (below several keV) because of inaccuracies in the QUICKE2 cross
sections. T : low-order Legendre polynomial representation of angular dis-
tributions u ¹ in the formulation results in anomalies at high energies
for low-atomic umber materials for quantities dependent on backward-
emitted electrons. For example, the QUICKE2 code gives negative values
for interface dose at the surface of mylar for photon energies of 600 keV
and up. An upgraded QUICKE code version would solve the angular distribu-
tion problem and extend cross section accuracy down to 1 keV (Ref. 2). The
analytical developments of Strickland (Ref. 3) for electron energies below
1 keV could also be employed to improve accuracy in the low-energy range.

The dipole moment computation employed here for cable effects is the
sum over energy of the product of the charge in each energy bin and its
mean penetration distance into a dielectric material. The material used
here is carbon, although electron ranges are relatively insensitive to
material for low atomic ~umbers (Ref. 14). Electrons are assumed to be
emitted normal to the surface for this computation. A better assumption
would be to use a distribution proportional to cos θ measured from the sur-
face normal (Ref. 15). This simplification introduces factor-of-two inac-
curacies in the absolute magnitude of the dipole moment; these inaccuracies
are quite uniform with photon energy and should not impair spectrum sensi-
tivity comparisons.

Algorithms for calculating the excitation parameters are given in
Table 5. Values for arbitrary spectra can be obtained by the expressions
once the terms for monoenergetic spectra are known. These are tabulated
for representative configurations below; ϕ_i represents the energy fluence

16

Table 5. SGEMP Excitation Term Algorithms for Arbitrary Spectra of Energy Fluence Φ_i versus Photon Energy i. (Lower-case symbols represent the parameter value computed for monoenergetic spectra of unit fluence.)

Dose $\qquad D = \sum_i \Phi_i \, d_i$

Electron Yield $\qquad Y = \sum_i \Phi_i \, y_i$

Average Velocity $\qquad \langle v \rangle = \dfrac{\sum\limits_i \Phi_i \, y_i}{\sum\limits_i \Phi_i \, y_i / \langle v \rangle_i}$

Average Energy $\qquad \langle \mathscr{E} \rangle = \dfrac{\sum\limits_i \Phi_i \, y_i \, \langle e \rangle_i}{\sum \Phi_i \, y_i}$

Dipole Moment $\qquad P = \sum \Phi_i \, p_i$

of the spectrum in bin i. The nonlinear cavity response algorithm is not so simple, and is presently in computer code form (see Section 5).

4.1 MONOENERGETIC SPECTRA

Excitation parameters are presented for monoenergetic photon spectra in Appendix A. Results are given in both graphic and tabular form. The tables may be used with the algorithms of Table 5 to obtain excitation parameter values for arbitrary spectra. A linear combination of contributions over all energies in the spectrum using the monoenergetic spectrum parameters as weighting factors gives the value corresponding to the arbitrary spectrum. An example employing the tables is treated in Section 6, and automated calculations employing them are described in Appendix D.

17

4.2 BLACKBODY SPECTRA

Excitation parameters are given here for blackbody spectra. The spectra and parameters are displayed as functions of blackbody temperature in Appendix B. Results for arbitrary combinations of blackbodies may be obtained by direct superposition of the parameter values in the same proportion as the fluences of the incident spectra.

5. RESPONSE PARAMETER CALCULATIONS

Satellite excitation parameters have been described above and tabulated in the appendices. The results are valid at all fluence levels, and are dependent only upon attenuation and emission materials for a given spectrum. The parameters chosen to meter satellite response to the excitations are described here. These differ from the excitation parameters in that they require additional geometry specification, and they depend upon photon flux rather than on total fluence. They also may become nonlinear at higher fluence levels due to space-charge-limiting. Thus, the response parameters are less general than excitation parameters, and they are not derivable from simple linear combinations of monoenergetic results in the space-charge-limited regime.

A first-order measure of satellite response variations due to varying photon spectrum may be achieved with a self-consistent solution of electron emission between grounded parallel plates. This solution resembles interior cavity response while remaining general and relatively simple to compute. In addition, results scale with the parameter Fd^2, where F is the photon flux and d is the diode spacing. Results are generalized in that they apply to a continuous range of spacings rather than to one specific case (see Ref. 1).

Response parameters employed here are the electric field at the front plate, the peak cavity potential, the transmitted current, and the electron charge dipole moment. The dipole moment presented here is the integral over the entire charge cloud of the product of the charge density times its distance from the emission face. Electron energy spectra are obtained from the QUICKE2 code. Angular variation of the electron number intensity is proportional to $\cos \theta$ where θ is measured from the surface normal. Charge is emitted from the forward plate. The treatment is equivalent to that in Reference 16, extended to arbitrary emission energy spectra between paralel plates.

Results for blackbody and blackbody combination spectra incident on aluminum plates are shown in Appendix C. The combination spectra plotted

were chosen from a larger set of combinations in the range 2 to 15 keV;
the ones chosen bracket the responses at virtually all levels.

Magnetic field estimates can be immediately made from the results
using the simple expression:

$$H_\phi = \frac{JR}{2} \, ,$$

where

H_ϕ = magnetic field (amp/m) ,

J = transmitted current density (amp/m^2) ,

R = diode radius (m) .

6. EXAMPLE USES OF THE PARAMETERS

Representative satellite excitation parameters for SGEMP have been determined and evaluated in previous sections of this report. Example uses of the parameters are discussed here. Excitation and response parameters for several bremsstrahlung photon spectra are computed and compared with values for a nominal spectrum. First, a sample illustration of the numerics is given.

6.1 SAMPLE COMPUTATION

A sample computation illustrating the use of the monoenergetic excitation parameters is shown in Figure 1. The electron yield from fiberglass behind a solar array is obtained for the spectrum shown by dividing it into energy bins of width 20 keV (the large bin width is used for illustrative purposes only, to reduce the numerical computation effort). The fluence in each energy bin and the electron yield corresponding to that energy are obtained (indicated by dots on the curves). The product of the two gives the electron yield due to photons in that energy bin. The sum over all bins gives the electron yield for the entire spectrum. These steps are illustrated mathematically by the relation:

$$Y = \sum_{i=1}^{N} \Phi_{\varepsilon_i} \Delta\varepsilon_i \, y_i$$

$$\simeq 20 \text{ keV} \times (2.7\times10^{-2} \times 2.0\times10^{-8} + 1.6\times10^{-2} \times 1.2\times10^{-8} + 4.5\times10^{-3}$$

$$\times 6.8\times10^{-9} + 8.7\times10^{-4} \times 4.5\times10^{-9})$$

$$\simeq 1.5 \times 10^{-8} \text{ C/cal} \qquad (\text{QUICKE} \ldots 1.4 \times 10^{-8} \text{ C/cal}) .$$

In this particular case, the results obtained with the large-energy bins correspond very well to results obtained with QUICKE2 using much finer bins. This approach applies to every parameter type using the corresponding algorithms of Table 5. Notice that we have assumed unit fluence to obtain the
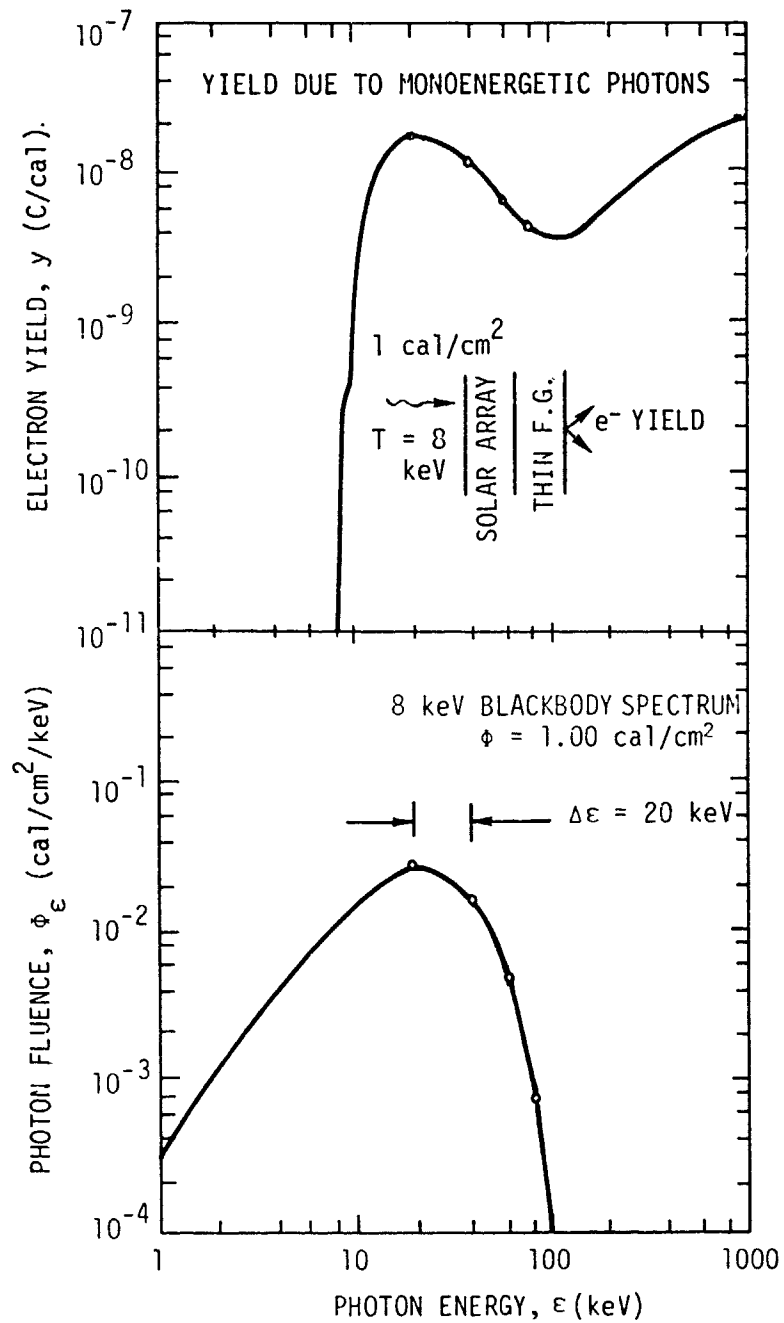
Figure 1. Sample calculation of electron yield due to an 8-keV blackbody incident on a solar array. Monoenergetic photon results are employed.

22

units C/cal for purposes of comparing spectra (see Figure 1). This normalization is employed for all excitation parameter results in this report.

6.2 BREMSSTRAHLUNG SPECTRUM EVALUATIONS

A subset of the parameters defined in previous sections has been evaluated for bremsstrahlung photon spectra in the range from 135 to 400 keV. The spectra are shown in Figure 2. The parameters used are indicated in Figure 3, below the spectrum profiles presented as ratios of the corresponding values for a 10-keV blackbody. The profiles diverge from unity as the bremsstrahlung energy increases. Examination of the 10-keV blackbody spectrum (see Appendix B) and the bremsstrahlungs corroborates this behavior. The lower-energy bremsstrahlung spectra are more similar in energy content to the 10-keV blackbody than the higher-energy bremsstrahlungs.

The cavity response to the incident bremsstrahlungs as a function of incident flux is shown in Figures 4 and 5. The spectra penetrate 3 mils of aluminum, emitting electrons to the interior from the first plate. Some space-charge-limiting is evident from the curve nonlinearities. For a diode spacing of 0.5 m and a pulse width of 30 nsec, space-charge-limiting begins at about 5×10^{-4} cal/cm^2.
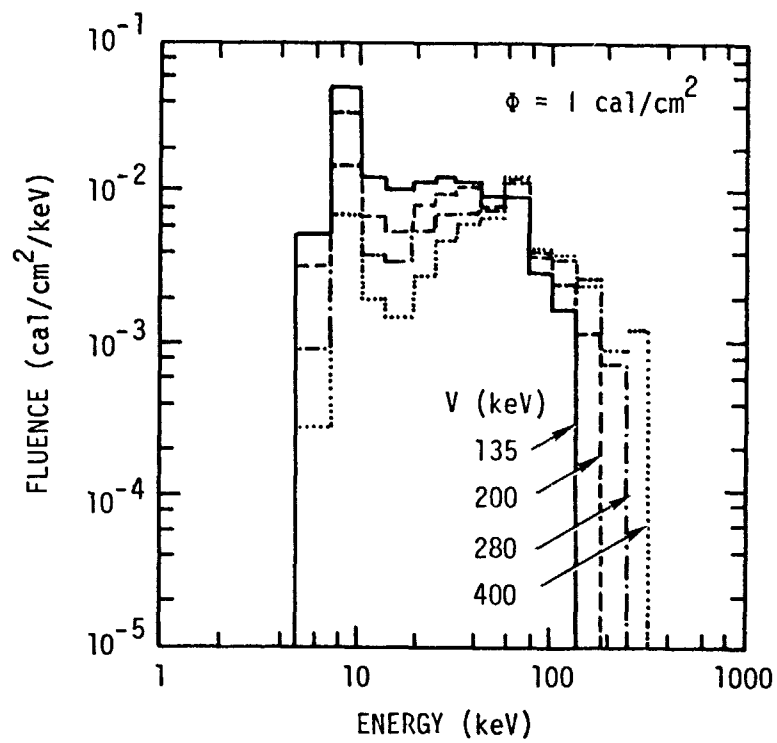
RE-01450

Figure 2. Bremsstrahlung photon spectra
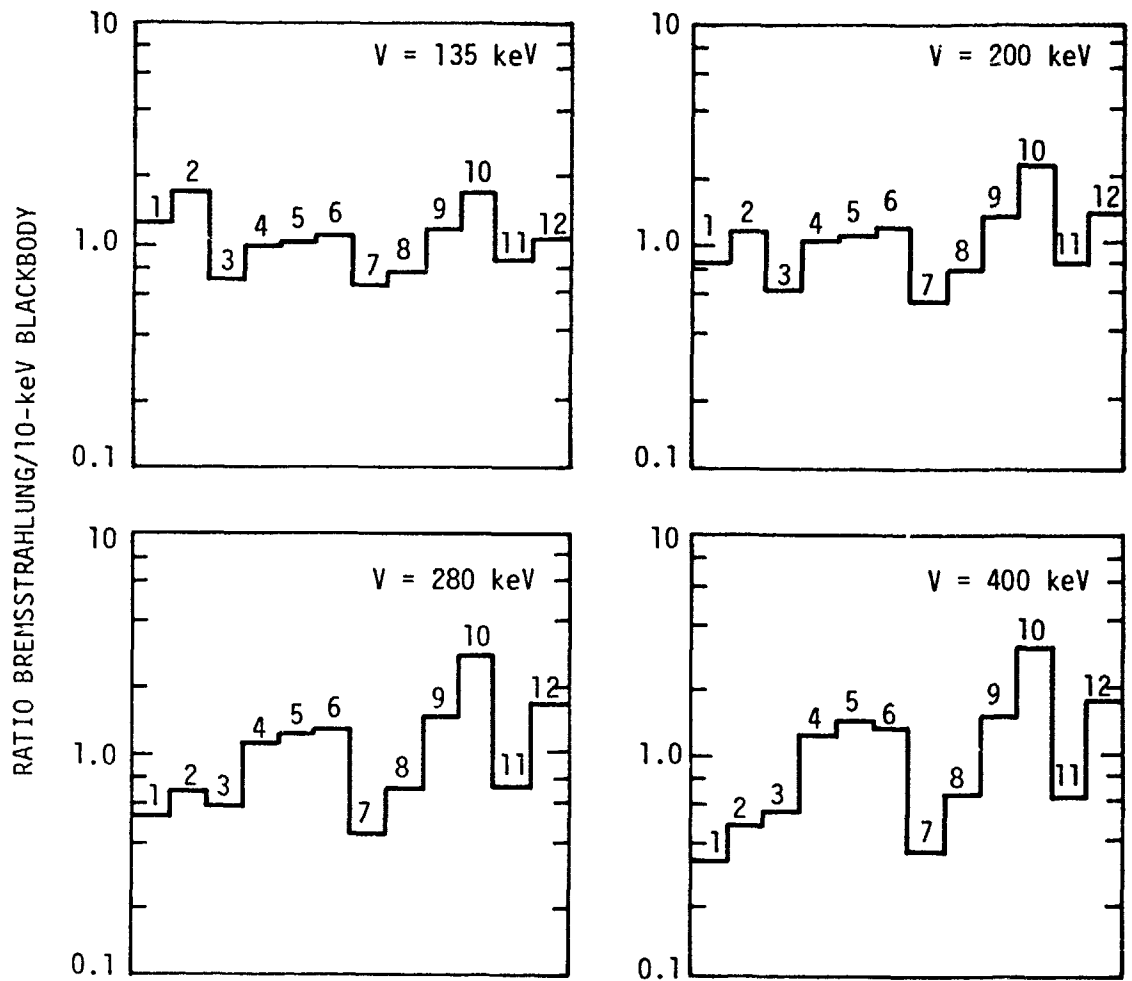
RE-01451   RESPONSE PARAMETERS

1 YIELD, 3-mil Al   7   YIELD, 20-mil Al BOX
2 YIELD, 10-mil MYLAR   8   DOSE INSIDE DEVICE HOUSING
3 YIELD, SOLAR ARRAY   9   DOSE RATIO Au/Si INSIDE HOUSING
4 <v> BEHIND 3-mil Al   10 DOSE IN SHIELDED BOX
5 YIELD, FORE/BACK BEHIND SOLAR ARRAY   11 CABLE YIELD (3 mils)
6 YIELD, HI/LO-Z BEHIND SOLAR ARRAY   12 CABLE DIPOLE MOMENT (3 mils)

Figure 3. Ratios of bremsstrahlung spectrum excitation parameters to corres-
           ponding values for a 10-keV blackbody. The bremsstrahlung voltage
           V is indicated for each figure.
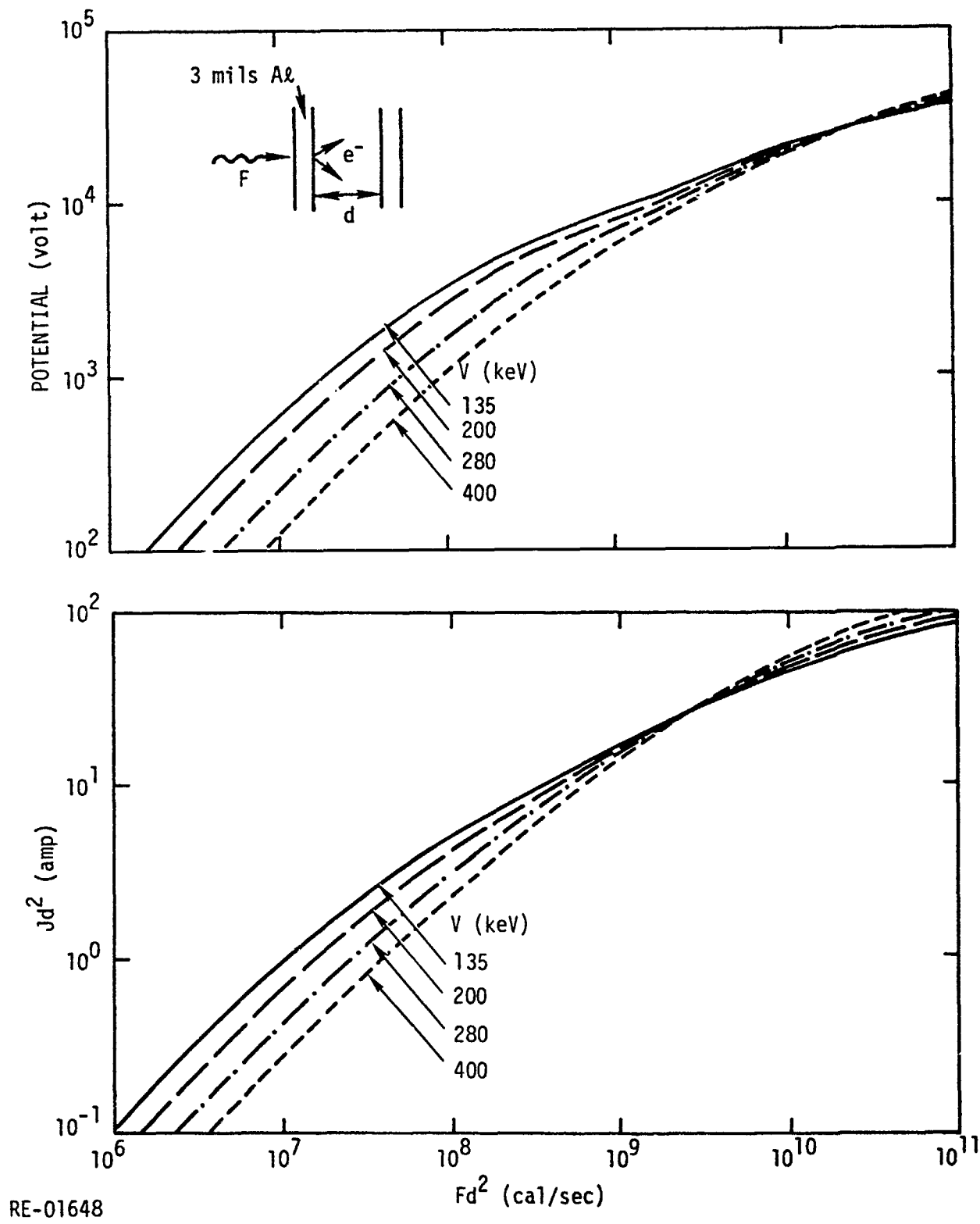
RE-01648

Figure 4. Diode potential and scaled current due to incident bremsstrahlung spectra of voltage V (keV). F is the photon flux, J is the electron current density, and d is the plate spacing.
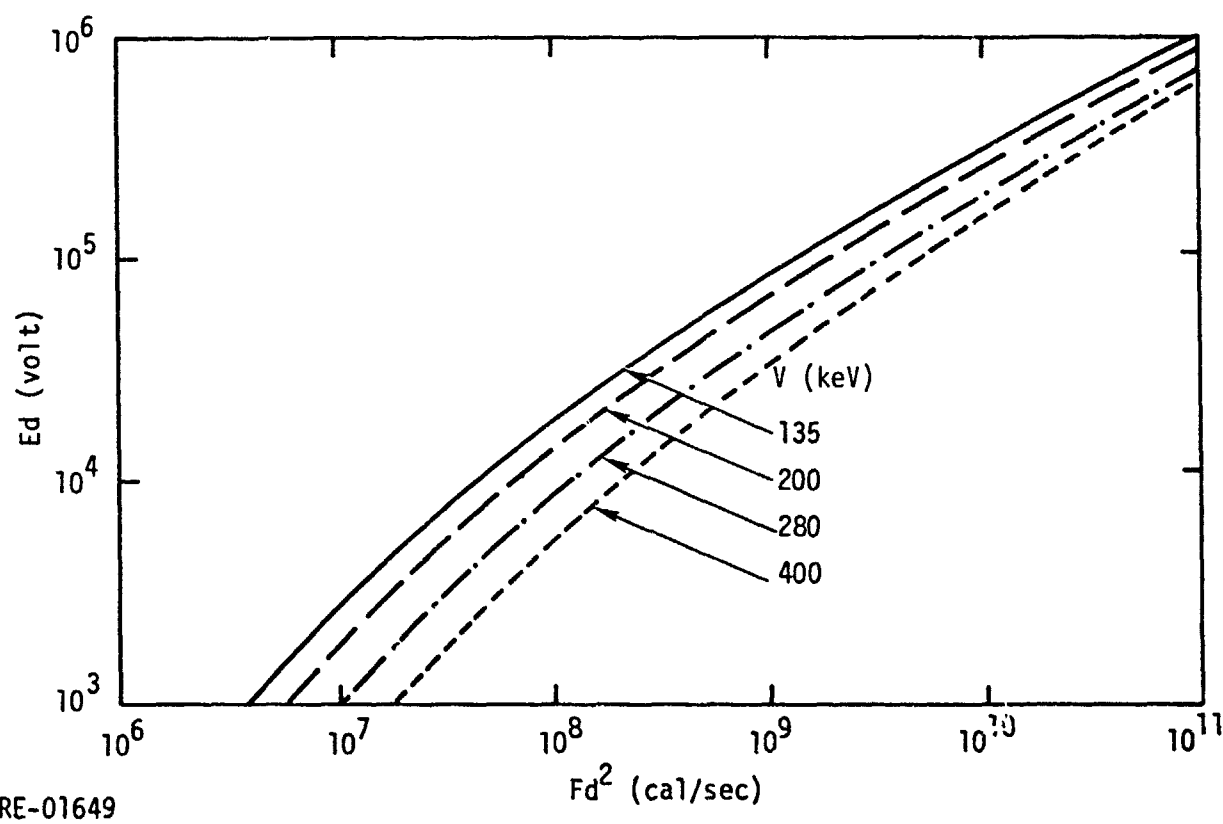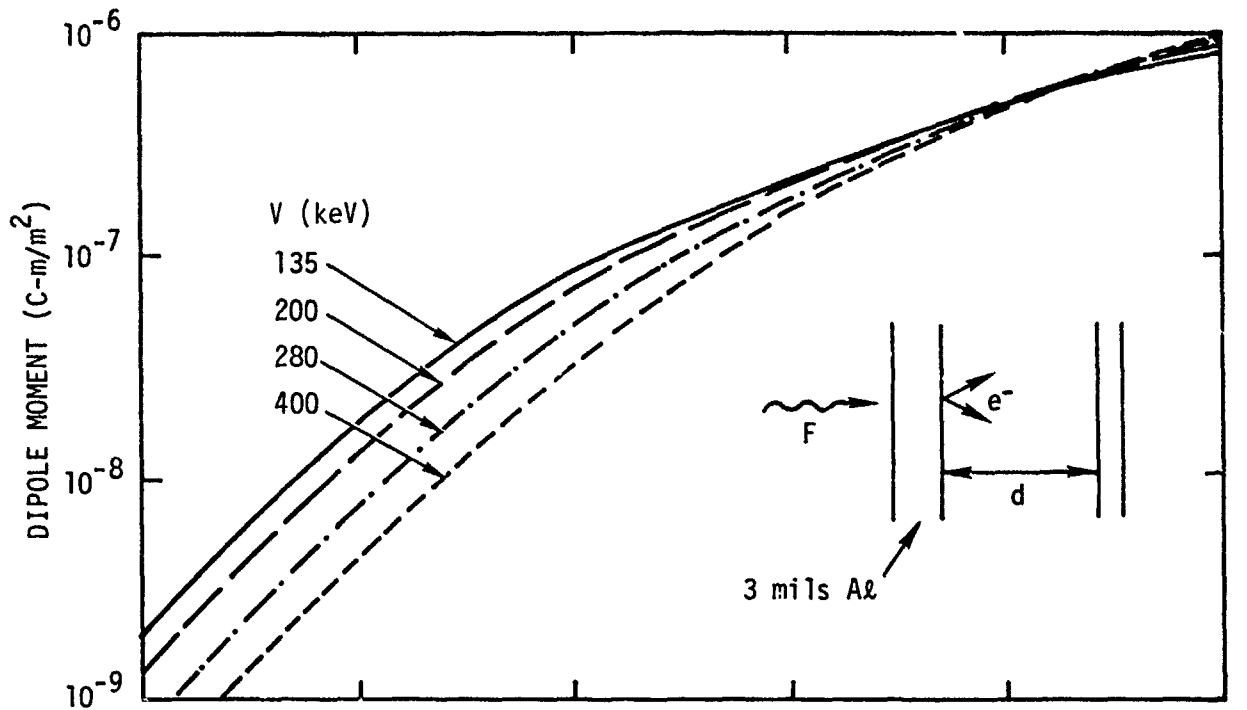
Figure 5. Dipole moment and scaled electric field at the front face of a diode due to incident bremsstrahlung spectra of voltage V (keV). F is the photon flux, E is the electric field, and d is the plate spacing.

RE-01649

27

REFERENCES

1. A. J. Woods and E. P. Wenaas, "Scaling Laws for SGEMP," IEEE Trans. Nucl. Sci. NS-23, No. 6, December 1976.

2. T. A. Dellin et al., "Second-Generation Analytical Photo-Compton Current Methods," IEEE Trans. Nucl. Sci. NS-22, No. 6, December 1975.

3. D. J. Strickland, "Soft X-ray Photoemission," IEEE Trans. Nucl. Sci. NS-24, No. 6, December 1977.

4. J. A. Wall and E. A. Burke, "Gamma-Dose Distributions At and Near the Interface of Different Materials," IEEE Trans. Nucl. Sci. NS-17, No. 6 (1970).

5. A. Wilson and D. E. Parks, "Body Current Response Scaling under High Fluence Conditions," IEEE Trans. Nucl. Sci. NS-23, No. 6, December 1976.

6. R. L. Fitzwilson et al., "Radiation-Induced Currents in Shielded Multi-Conductor and Semirigid Cables," IEEE Trans. Nucl. Sci. NS-21, No. 6, December 1974.

7. E. P. dePlomb, "Analytical Modeling and Experimental Testing of Pressure Effects in Small Cavities Coupled to Circuitry," IEEE Trans. Nucl. Sci. NS-21, No. 6, December 1974.

8. F. Hai et al., "Measured and Predicted Radiation-Induced Currents in Semirigid Coaxial Cables," IEEE Trans. Nucl. Sci. NS-24, No. 6, December 1977.

9. E. P. Wenaas and S. H. Rogers, "Effects of Dielectrics on the SGEMP Response of Satellite Structures," AFWL-TR-75-233, Vol. 1, July 1975.

10. W. L. Chadsey, "X-Ray-Produced Charge Deposition and Dose in Dielectrics Near Interfaces Including Space-Charge Field and Conductivity Effects," IEEE Trans. Nucl. Sci. NS-21, No. 6, December 1974.

11. E. P. Wenaas and A. J. Woods, "Effects of Backscattered Electrons on SGEMP Response," IEEE Trans. Nucl. Sci. NS-23, No. 6, December 1976.

12. S. Brucker, TRW, private communication, October 1977.

13. S. H. Rogers and A. J. Woods, "Multiple-Plate Modification of the QUICKE2 Electron Emission Code," DNA 4064T, June 1976.

14. M. J. Berger and S. M. Seltzer, "Tables of Energy Losses and Ranges of Electrons and Positrons," NASA SP-3012 (1964).

15. W. L. Chadsey and C. W. Wilson, "X-Ray Photoemission," HDL-CR-75-138-1, September 1975.

16. N. J. Carron and C. L. Longmire, "On the Structure of the Steady-State Space-Charge-Limited Boundary Layer in One Dimension," DNA 2938T, November 1975.

APPENDIX A

EXCITATION PARAMETER RESULTS
FOR MONOENERGETIC SPECTRA
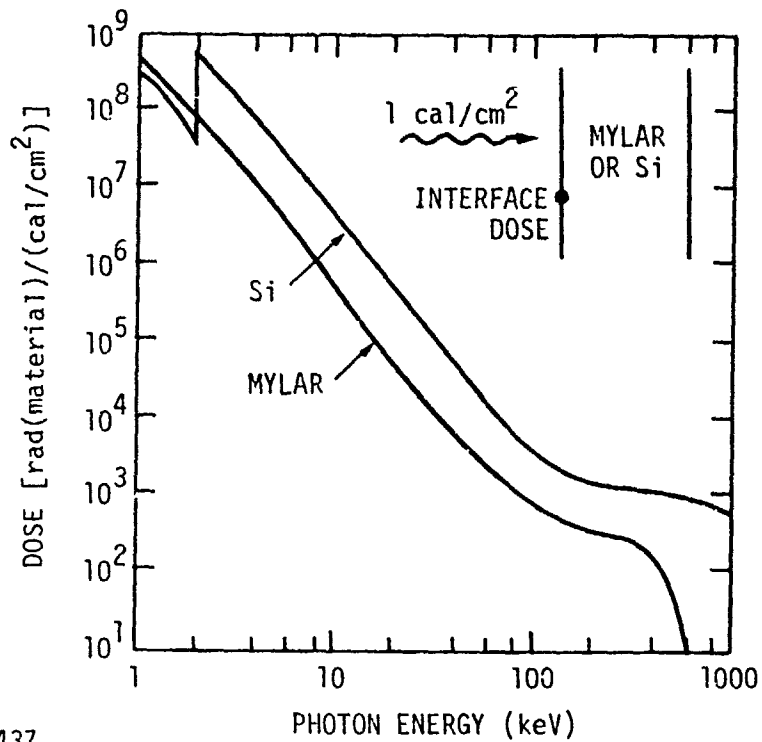
RE-01437

PHOTON ENERGY (keV)	INTERFACE DOSE		PHOTON ENERGY (keV)	INTERFACE DOSE	
	[rad(Mylar)]	[rad(Si)]		[rad(Mylar)]	[rad(Si)]
2	8.467×10^7	5.497×10^8	90	9.893×10^2	5.180×10^3
5	5.065×10^6	4.082×10^7	100	7.834×10^2	4.018×10^3
10	5.382×10^5	4.873×10^6	125	5.363×10^2	2.589×10^3
15	1.388×10^5	1.385×10^6	150	4.286×10^2	1.876×10^3
20	5.248×10^4	5.588×10^5	200	3.579×10^2	1.384×10^3
30	1.409×10^4	1.529×10^5	300	2.704×10^2	1.175×10^3
40	6.155×10^3	5.989×10^4	400	1.690×10^2	1.097×10^3
50	3.580×10^3	2.918×10^4	500	5.828×10^1	1.019×10^3
60	2.422×10^3	1.643×10^4	600	-	9.347×10^2
70	1.746×10^3	1.031×10^4	800	-	7.604×10^2
80	1.296×10^3	7.059×10^3	1000	-	5.92×10^2

Figure A-1.   Interface dose at the surface of dielectric materials
due to monoenergetic photons incident at 1 cal/cm^2

30
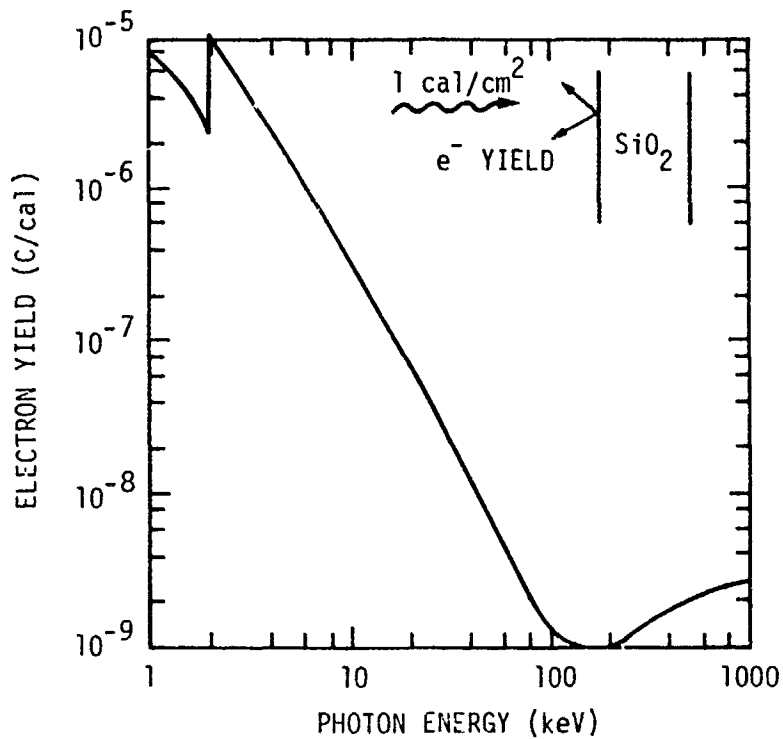
RE-01438

PHOTON ENERGY (keV)	ELECTRON YIELD (C/cal)	PHOTON ENERGY (keV)	ELECTRON YIELD (C/cal)
2	1.098×10^{-5}	90	1.544×10^{-9}
5	1.202×10^{-6}	100	1.242×10^{-9}
10	3.092×10^{-7}	125	9.152×10^{-10}
15	1.299×10^{-7}	150	8.181×10^{-10}
20	6.707×10^{-8}	200	9.226×10^{-10}
30	2.484×10^{-8}	300	1.348×10^{-9}
40	1.198×10^{-8}	400	1.747×10^{-9}
50	6.681×10^{-9}	500	2.067×10^{-9}
60	4.260×10^{-9}	600	2.308×10^{-9}
70	2.843×10^{-9}	800	2.605×10^{-9}
80	2.031×10^{-9}	1000	2.750×10^{-9}

Figure A-2. Reverse-emitted electron yield at the surface of quartz due to monoenergetic photons incident at 1 cal/cm²
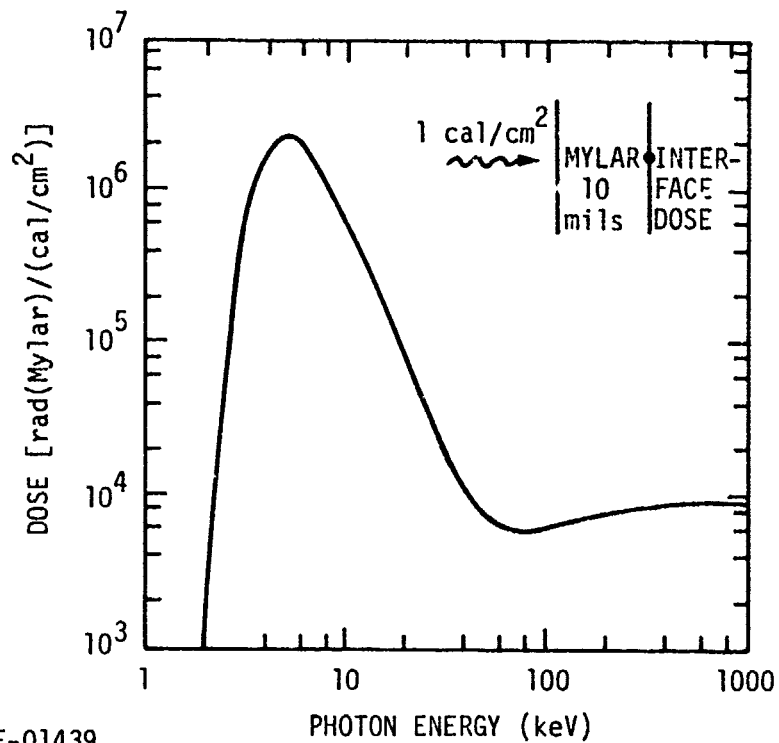
RE-01439

PHOTON ENERGY (keV)	INTERFACE DOSE [rad(Mylar)]	PHOTON ENERGY (keV)	INTERFACE DOSE [rad(Mylar)]
2	3.949×10^1	90	6.304×10^3
5	2.227×10^6	100	6.504×10^3
10	6.110×10^5	125	7.019×10^3
15	1.810×10^5	150	7.490×10^3
20	7.385×10^4	200	8.202×10^3
30	2.232×10^4	300	9.040×10^3
40	1.105×10^4	400	9.454×10^3
50	7.600×10^3	500	9.656×10^3
60	6.447×10^3	600	9.745×10^3
70	6.132×10^3	800	9.740×10^3
80	6.152×10^3	1000	9.613×10^3

Figure A-3.   Interface dose behind thermal blanket due to monoenergetic photons incident at 1 cal/cm^2
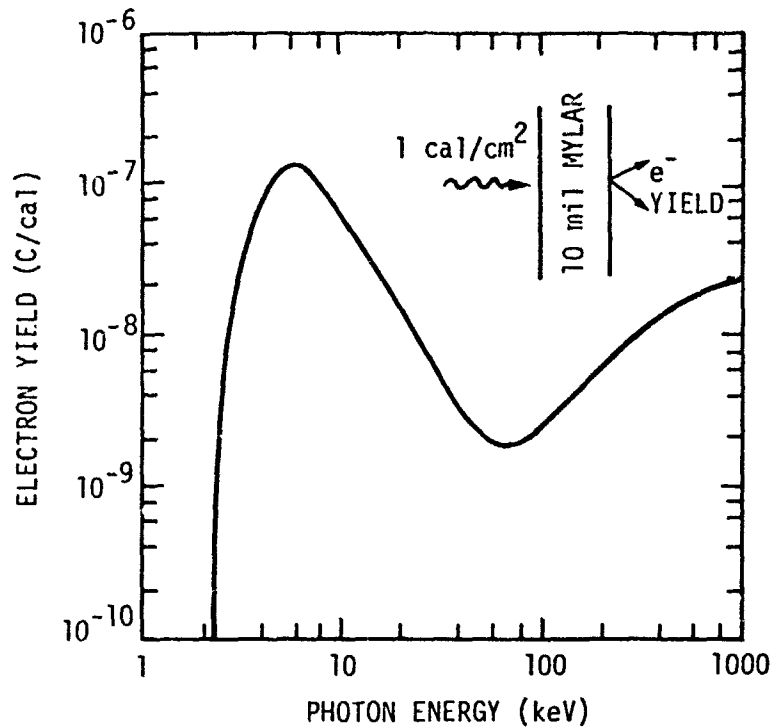
RE-01215A

PHOTON ENERGY (keV)	ELECTRON YIELD (C/cal)	PHOTON ENERGY (keV)	ELECTRON YIELD (C/cal)
2	-	90	2.067×10^{-9}
5	2.260×10^{-7}	100	2.298×10^{-9}
10	7.178×10^{-8}	125	3.119×10^{-9}
15	2.962×10^{-8}	150	4.028×10^{-9}
20	1.563×10^{-8}	200	6.112×10^{-9}
30	6.222×10^{-9}	300	1.026×10^{-8}
40	3.409×10^{-9}	400	1.391×10^{-8}
50	2.342×10^{-9}	500	1.698×10^{-8}
60	1.931×10^{-9}	600	1.945×10^{-8}
70	1.817×10^{-9}	800	2.316×10^{-8}
80	1.882×10^{-9}	1000	2.554×10^{-8}

Figure A-4. Electron yield behind thermal blanket due to monoenergetic photons incident at 1 cal/cm^2
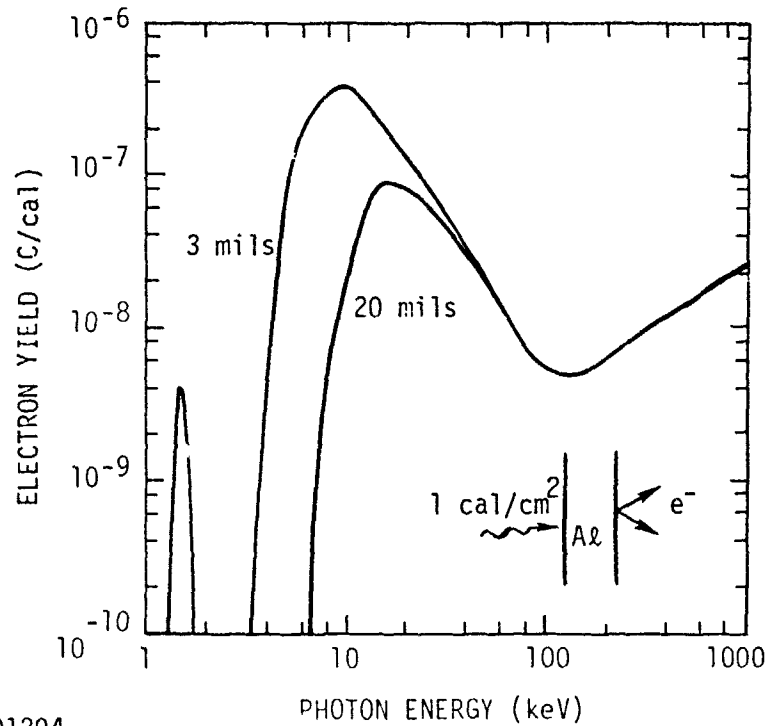
RE-01204

PHOTON ENERGY (keV)	ELECTRON YIELD (C/cal)		PHOTON ENERGY (keV)	ELECTRON YIELD (C/cal)	
	3 mils	20 mils		3 mils	20 mils
2	-	-	90	6.510×10^{-9}	6.372×10^{-9}
5	5.00×10^{-8}	-	100	5.653×10^{-9}	5.542×10^{-9}
10	3.558×10^{-7}	1.797×10^{-8}	125	4.921×10^{-9}	4.835×10^{-9}
15	2.305×10^{-7}	9.154×10^{-8}	150	4.913×10^{-9}	4.835×10^{-9}
20	1.399×10^{-7}	9.410×10^{-8}	200	6.052×10^{-9}	5.967×10^{-9}
30	6.213×10^{-8}	5.408×10^{-8}	300	9.174×10^{-9}	9.062×10^{-9}
40	3.269×10^{-8}	3.060×10^{-8}	400	1.214×10^{-8}	1.202×10^{-8}
50	2.108×10^{-8}	2.020×10^{-8}	500	1.467×10^{-8}	1.451×10^{-8}
60	1.405×10^{-8}	1.360×10^{-8}	600	1.670×10^{-8}	1.653×10^{-8}
70	1.020×10^{-8}	9.930×10^{-9}	800	1.977×10^{-8}	1.959×10^{-8}
80	7.389×10^{-9}	7.708×10^{-9}	1000	2.173×10^{-8}	2.155×10^{-8}

Figure A-5. Forward-emitted electron yield from aluminum after penetration of 3 and 20 mils aluminum by monoenergetic photons

34

RE-01217A
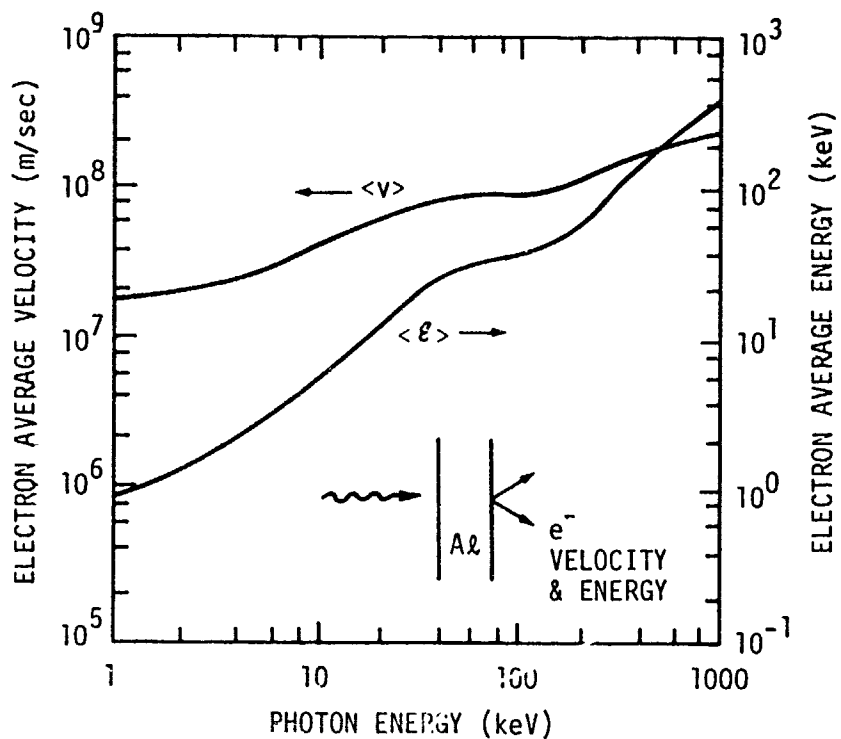
PHOTON ENERGY (keV)	ELECTRON AVERAGE VELOCITY (m/sec)	ELECTRON AVERAGE ENERGY (keV)	PHOTON ENERGY (keV)	ELECTRON AVERAGE VELOCITY (m/sec)	ELECTRON AVERAGE ENERGY (keV)
2	2.10×10^7	1.28	90	1.05×10^8	5.23×10^1
5	2.83×10^7	2.52	100	1.04×10^8	5.37×10^1
10	4.24×10^7	5.94	125	1.04×10^8	5.39×10^1
15	5.38×10^7	9.55	150	1.07×10^8	5.38×10^1
20	6.28×10^7	1.32×10^1	200	1.26×10^8	6.17×10^1
30	7.71×10^7	2.04×10^1	300	1.48×10^8	9.61×10^1
40	8.74×10^7	2.71×10^1	400	1.71×10^8	1.40×10^2
50	9.64×10^7	3.45×10^1	500	1.89×10^8	1.86×10^2
60	1.01×10^8	4.05×10^1	600	2.03×10^8	2.33×10^2
70	1.05×10^8	4.58×10^1	800	2.23×10^8	3.31×10^2
80	1.05×10^8	4.98×10^1	1000	2.37×10^8	4.28×10^2

Figure A-6. Average velocity and energy of electrons emitted from aluminum due to monoenergetic photons incident

RE-01218

PHOTON ENERGY (keV)	ELECTRON YIELD (C/cal)		PHOTON ENERGY (keV)	ELECTRON YIELD (C/cal)	
	FORWARD	REVERSE		FORWARD	REVERSE
2	–	–	90	3.872×10^{-9}	1.055×10^{-9}
5	1.196×10^{-18}	9.607×10^{-19}	100	3.663×10^{-9}	8.805×10^{-10}
10	4.916×10^{-10}	3.592×10^{-10}	125	3.802×10^{-9}	7.025×10^{-10}
15	1.385×10^{-8}	9.239×10^{-9}	150	4.273×10^{-9}	6.704×10^{-10}
20	2.018×10^{-8}	1.252×10^{-8}	200	5.862×10^{-9}	8.086×10^{-10}
30	1.760×10^{-8}	9.629×10^{-9}	300	9.429×10^{-9}	1.226×10^{-9}
40	1.171×10^{-8}	5.818×10^{-9}	400	1.258×10^{-8}	1.590×10^{-9}
50	8.770×10^{-9}	3.932×10^{-9}	500	1.559×10^{-8}	1.929×10^{-9}
60	6.816×10^{-9}	2.707×10^{-9}	600	1.785×10^{-8}	2.162×10^{-9}
70	5.358×10^{-9}	1.897×10^{-9}	800	2.116×10^{-8}	2.444×10^{-9}
80	4.492×10^{-9}	1.403×10^{-9}	1000	2.328×10^{-8}	2.582×10^{-9}

Figure A-7. Electron yields from fiberglass behind solar array due to monoenergetic photons incident at 1 cal/cm^2

36
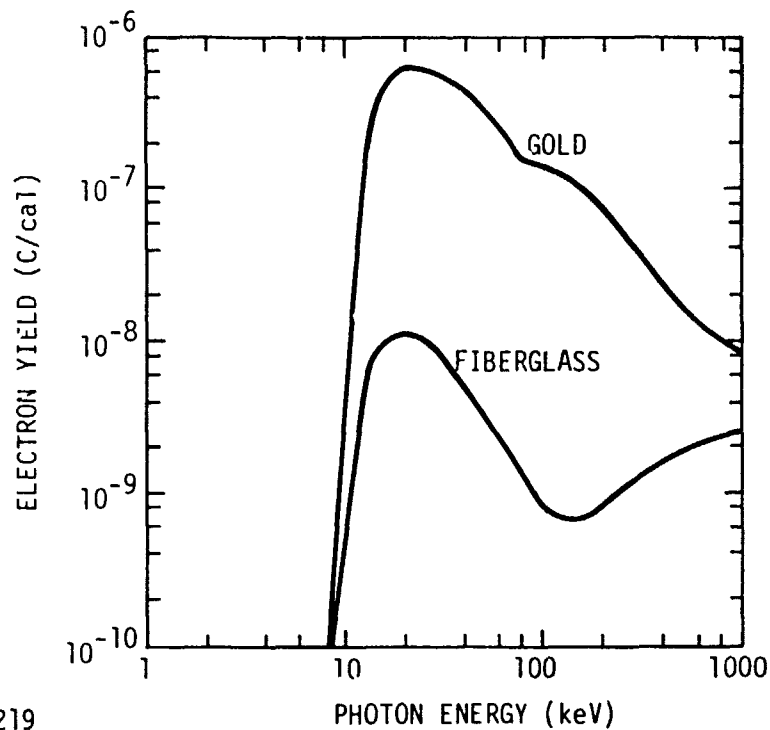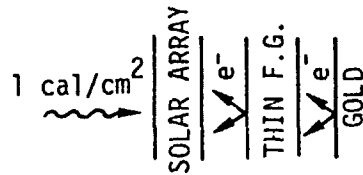
RE-01219
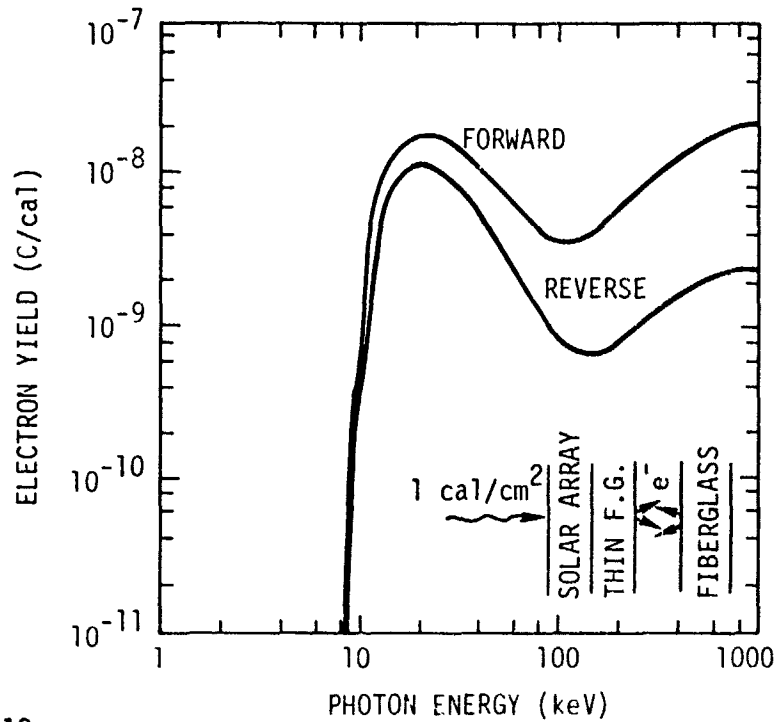
PHOTON ENERGY (keV)	ELECTRON YIELD (C/cal)		PHOTON ENERGY (keV)	ELECTRON YIELD (C/cal)	
	GOLD	FIBERGLASS		GOLD	FIBERGLASS
2	-	-	90	1.590×10^{-7}	1.055×10^{-9}
5	1.284×10^{-17}	9.607×10^{-19}	100	1.532×10^{-7}	8.805×10^{-10}
10	6.597×10^{-9}	3.592×10^{-10}	125	1.291×10^{-7}	7.025×10^{-10}
15	4.012×10^{-7}	9.239×10^{-9}	150	1.082×10^{-7}	6.704×10^{-10}
20	6.680×10^{-7}	1.252×10^{-8}	200	7.395×10^{-8}	8.086×10^{-10}
30	6.064×10^{-7}	9.629×10^{-9}	300	3.839×10^{-8}	1.226×10^{-9}
40	4.358×10^{-7}	5.818×10^{-9}	400	2.383×10^{-8}	1.590×10^{-9}
50	3.363×10^{-7}	3.932×10^{-9}	500	1.748×10^{-8}	1.929×10^{-9}
60	2.588×10^{-7}	2.707×10^{-9}	600	1.383×10^{-8}	2.162×10^{-9}
70	1.997×10^{-7}	1.897×10^{-9}	800	1.022×10^{-8}	2.444×10^{-9}
80	1.500×10^{-7}	1.403×10^{-9}	1000	8.565×10^{-9}	2.582×10^{-9}

Figure A-8. Reverse-emitted electron yields from gold and fiberglass behind solar array due to monoenergetic photons incident

37
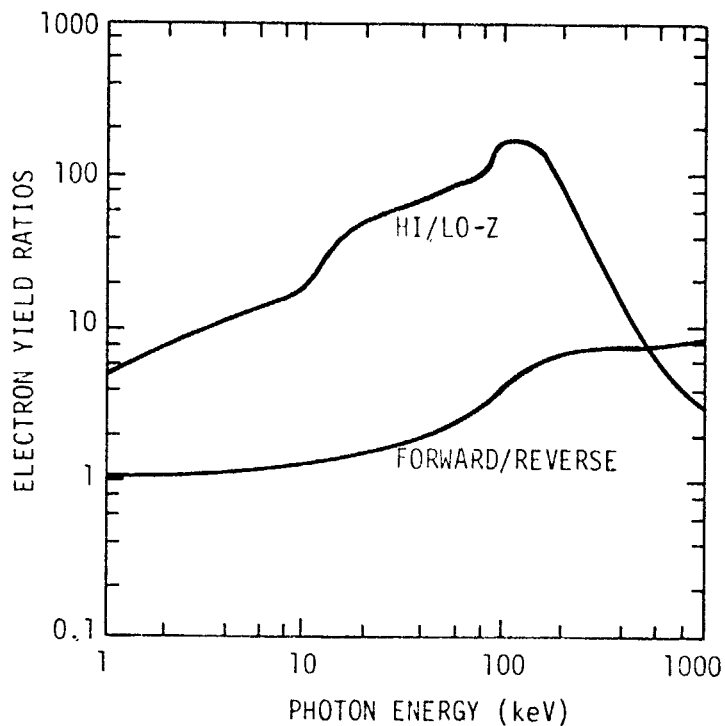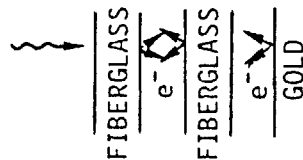
RE-01220

PHOTON ENERGY (keV)	ELECTRON YIELD RATIOS		PHOTON ENERGY (keV)	ELECTRON YIELD RATIOS	
	FORWARD/ REVERSE	HIGH/ LOW-Z		FORWARD/ REVERSE	HIGH/ LOW-Z
2	1.100	5.00	90	3.669	150.6
5	1.245	13.37	100	4.160	174.0
10	1.369	18.36	125	5.411	183.8
15	1.499	43.43	150	6.373	161.4
20	1.612	53.37	200	7.250	91.45
30	1.828	62.98	300	7.691	31.31
40	2.012	74.91	400	7.910	14.99
50	2.230	85.53	500	8.082	9.063
60	2.518	95 60	600	8.256	6.398
70	2.824	105.3	800	8.660	4.184
80	3.202	106.9	1000	9.018	3.318

Figure A-9. Electron emission ratios for monoenergetic photons. The high-to-low-Z ratio is for reverse emission from gold compared to fiberglass, and the forward-to-reverse ratio is for aluminum.

38
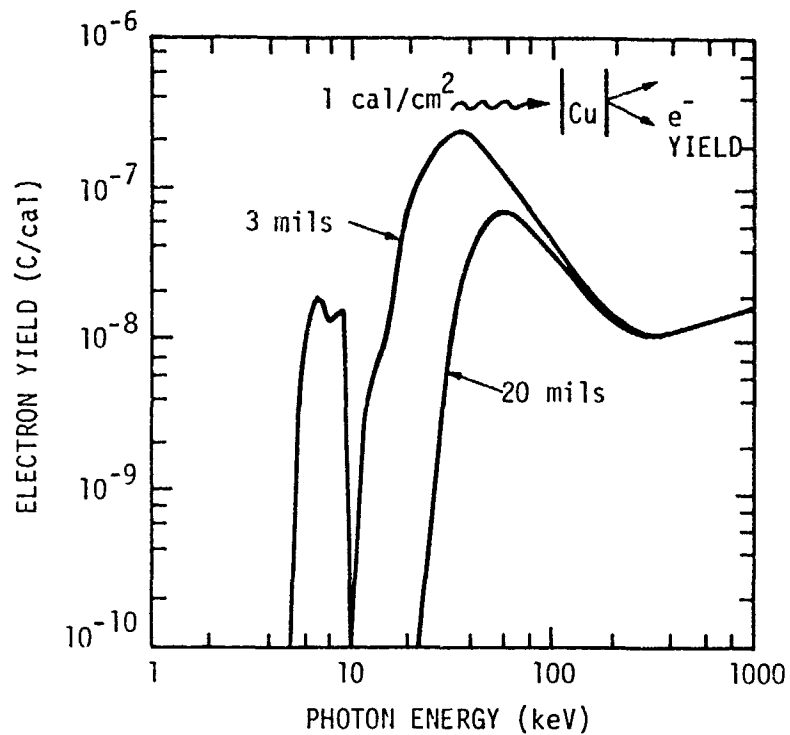
RE-01225A

PHOTON ENERGY (keV)	ELECTRON YIELD (C/cal)		PHOTON ENERGY (keV)	ELECTRON YIELD (C/cal)	
	3 mils	20 mils		3 mils	20 mils
2	–	–	90	5.873×10^{-8}	4.705×10^{-8}
5	9.564×10^{-12}	–	100	5.070×10^{-8}	4.259×10^{-8}
10	1.257×10^{-12}	–	125	3.283×10^{-8}	2.923×10^{-8}
15	1.242×10^{-8}	–	150	2.395×10^{-8}	2.195×10^{-8}
20	9.770×10^{-8}	2.778×10^{-13}	200	1.501×10^{-8}	1.414×10^{-8}
30	2.325×10^{-7}	6.218×10^{-9}	300	1.154×10^{-8}	1.106×10^{-8}
40	2.291×10^{-7}	3.637×10^{-8}	400	1.170×10^{-8}	1.131×10^{-8}
50	1.691×10^{-7}	6.280×10^{-8}	500	1.279×10^{-8}	1.234×10^{-8}
60	1.279×10^{-7}	6.991×10^{-8}	600	1.388×10^{-8}	1.341×10^{-8}
70	1.008×10^{-7}	6.707×10^{-8}	800	1.580×10^{-8}	1.535×10^{-8}
80	7.621×10^{-8}	5.704×10^{-8}	1000	1.713×10^{-8}	1.668×10^{-8}

Figure A-10. Electron yield inside cables of shield thicknesses 3 and 20 mils due to monoenergetic photons incident at 1 cal/cm^2
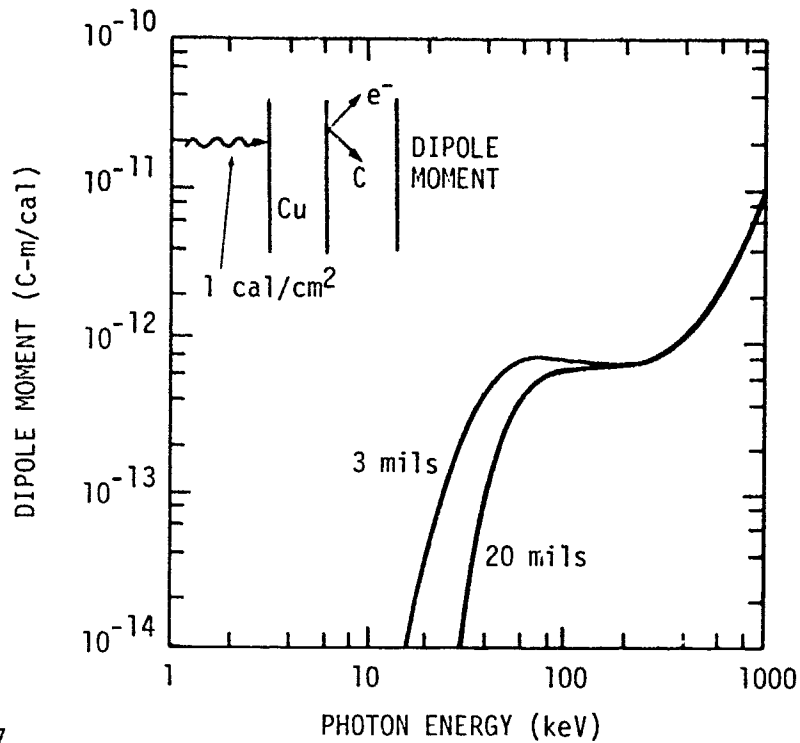
RE-01457

PHOTON ENERGY (keV)	DIPOLE MOMENT (C-m/cal)		PHOTON ENERGY (keV)	DIPOLE MOMENT (C-m/cal)	
	3 mils	20 mils		3 mils	20 mils
2	–	–	90	7.32×10^{-13}	5.87×10^{-13}
5	–	–	100	8.00×10^{-13}	6.76×10^{-13}
10	–	–	125	7.56×10^{-13}	6.76×10^{-13}
15	2.57×10^{-15}	–	150	7.81×10^{-13}	7.13×10^{-13}
20	3.98×10^{-14}	–	200	7.07×10^{-13}	6.63×10^{-13}
30	2.68×10^{-13}	7.07×10^{-15}	300	7.75×10^{-13}	8.00×10^{-13}
40	5.35×10^{-13}	8.49×10^{-14}	400	1.15×10^{-12}	1.12×10^{-12}
50	6.39×10^{-13}	2.37×10^{-13}	500	1.79×10^{-12}	1.72×10^{-12}
60	7.19×10^{-13}	3.94×10^{-13}	600	2.72×10^{-12}	2.63×10^{-12}
70	7.94×10^{-13}	5.29×10^{-13}	800	5.57×10^{-12}	5.54×10^{-12}
80	7.63×10^{-13}	5.72×10^{-13}	1000	9.61×10^{-12}	9.30×10^{-12}

Figure A-11. Dipole moment inside cable dielectric due to monoenergetic photons incident at 1 cal/cm². Copper shield thicknesses are indicated beside the curves.

RE-01440

PHOTON ENERGY (keV)	BULK DOSE [rad(Au)]	BULK DOSE [rad(Si)]	PHOTON ENERGY (keV)	BULK DOSE [rad(Au)]	BULK DOSE [rad(Si)]
2	–	–	90	8.843×10^5	2.176×10^4
5	–	–	100	8.105×10^5	1.813×10^4
10	1.368×10^6	3.988×10^5	125	5.962×10^5	1.412×10^4
15	1.818×10^7	1.366×10^6	150	4.218×10^5	1.249×10^4
20	1.709×10^7	1.057×10^6	200	2.324×10^5	1.186×10^4
30	8.313×10^6	4.141×10^5	300	9.701×10^4	1.208×10^4
40	4.241×10^6	1.857×10^5	400	5.444×10^4	1.230×10^4
50	2.404×10^6	9.703×10^4	500	3.672×10^4	1.234×10^4
60	1.494×10^6	5.778×10^4	600	2.779×10^4	1.228×10^4
70	9.946×10^5	3.829×10^4	800	1.937×10^4	1.198×10^4
80	7.178×10^5	2.780×10^4	1000	1.553×10^4	1.159×10^4

Figure A-12. Bulk dose inside box due to monoenergetic photons incident at 1 cal/cm^2

41

RE-01222A
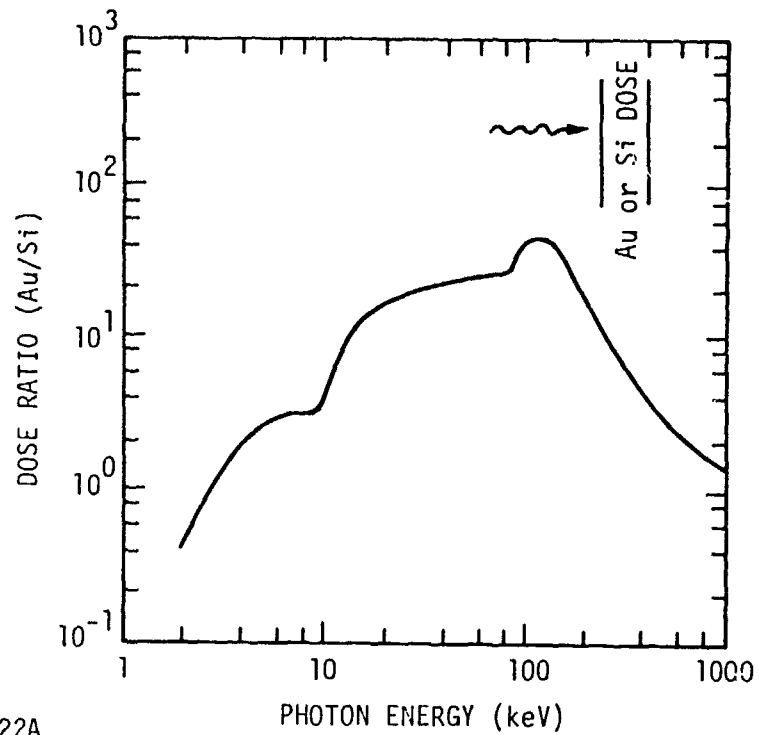
PHOTON ENERGY (keV)	DOSE RATIO (Au/Si)	PHOTON ENERGY (keV)	DOSE RATIO (Au/Si)
2	3.970×10^{-1}	90	4.064×10^{1}
5	2.702×10^{0}	100	4.469×10^{1}
10	3.446×10^{0}	125	4.224×10^{1}
15	1.331×10^{1}	150	3.377×10^{1}
20	1.617×10^{1}	200	1.960×10^{1}
30	2.008×10^{1}	300	8.028×10^{0}
40	2.284×10^{1}	400	4.428×10^{0}
50	2.478×10^{1}	500	2.976×10^{0}
60	2.585×10^{1}	600	2.264×10^{0}
70	2.598×10^{1}	800	1.617×10^{0}
80	2.582×10^{1}	1000	1.340×10^{0}

Figure A-13. Bulk dose ratio in gold compared to silicon for mono-
energetic photons
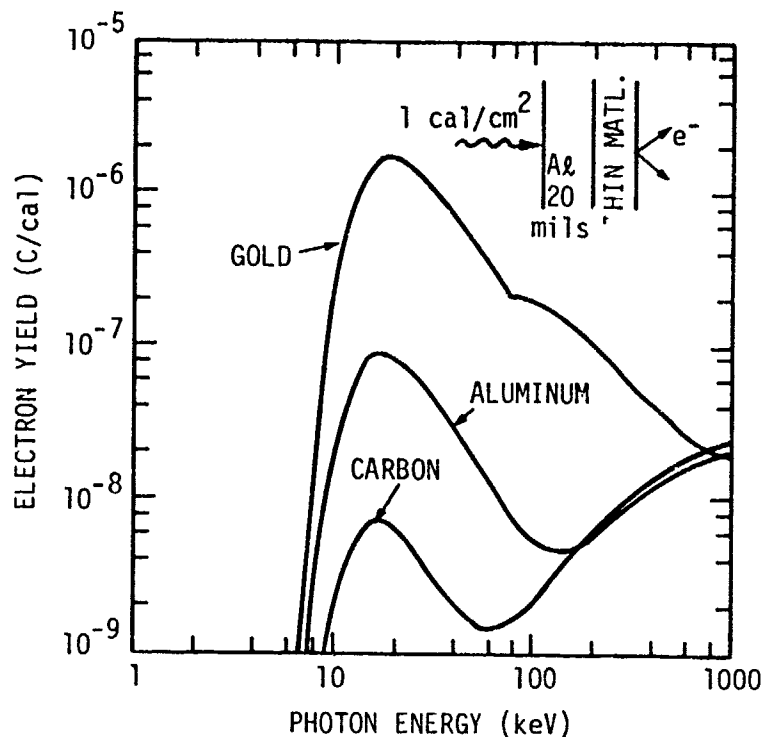
42

RE-01441

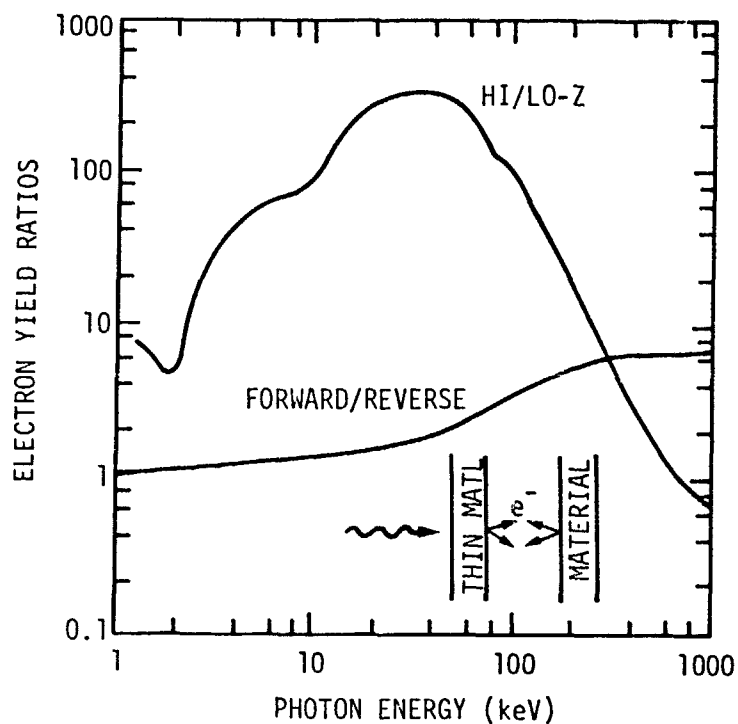| PHOTON ENERGY (keV)	ELECTRON YIELD (C/cal)			PHOTON ENERGY (keV)	ELECTRON YIELD (C/cal)		
	Carbon	Aluminum	Gold		Carbon	Aluminum	Gold
2	-	-	-	90	1.882×10^{-9}	6.372×10^{-9}	2.235×10^{-7}
5	-	-	-	100	2.152×10^{-9}	5.542×10^{-9}	2.079×10^{-7}
10	1.705×10^{-9}	1.797×10^{-8}	1.496×10^{-7}	125	3.026×10^{-9}	4.835×10^{-9}	1.786×10^{-7}
15	7.255×10^{-9}	9.154×10^{-8}	1.511×10^{-6}	150	3.965×10^{-9}	4.835×10^{-9}	1.553×10^{-7}
20	6.618×10^{-9}	9.410×10^{-8}	1.889×10^{-6}	200	6.078×10^{-9}	5.967×10^{-9}	1.078×10^{-7}
30	3.525×10^{-9}	5.408×10^{-8}	1.171×10^{-6}	300	1.025×10^{-8}	9.062×10^{-9}	6.215×10^{-8}
40	2.158×10^{-9}	3.060×10^{-8}	7.529×10^{-7}	400	1.396×10^{-8}	1.202×10^{-8}	4.125×10^{-8}
50	1.620×10^{-9}	2.020×10^{-8}	5.164×10^{-7}	500	1.704×10^{-8}	1.451×10^{-8}	3.467×10^{-8}
60	1.459×10^{-9}	1.360×10^{-8}	3.864×10^{-7}	600	1.954×10^{-8}	1.653×10^{-8}	2.651×10^{-8}
70	1.487×10^{-9}	9.930×10^{-9}	2.919×10^{-7}	800	2.331×10^{-8}	1.959×10^{-8}	2.099×10^{-8}
80	1.640×10^{-9}	7.708×10^{-9}	2.095×10^{-7}	1000	2.574×10^{-8}	2.155×10^{-8}	1.875×10^{-8}

Figure A-14.　Electron yields forward-emitted from materials inside box due to monoenergetic photons incident at 1 cal/cm^2
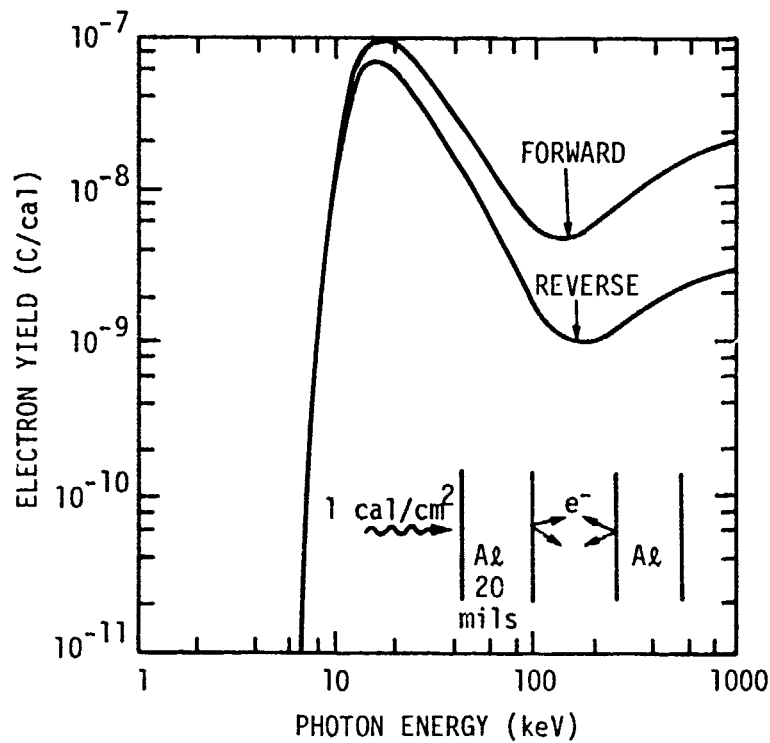
RE-01442

PHOTON ENERGY (keV)	ELECTRON YIELD (C/cal)		PHOTON ENERGY (keV)	ELECTRON YIELD (C/cal)	
	FORWARD	REVERSE		FORWARD	REVERSE
2	-	-	90	6.372×10^{-9}	2.178×10^{-9}
5	-	-	100	5.542×10^{-9}	1.724×10^{-9}
10	1.797×10^{-8}	1.359×10^{-8}	125	4.835×10^{-9}	1.204×10^{-9}
15	9.154×10^{-8}	6.381×10^{-8}	150	4.835×10^{-9}	1.015×10^{-9}
20	9.410×10^{-8}	6.159×10^{-8}	200	5.967×10^{-9}	1.065×10^{-9}
30	5.408×10^{-8}	3.172×10^{-8}	300	9.062×10^{-9}	1.495×10^{-9}
40	3.060×10^{-8}	1.655×10^{-8}	400	1.202×10^{-8}	1.922×10^{-9}
50	2.020×10^{-8}	9.882×10^{-9}	500	1.451×10^{-8}	2.271×10^{-9}
60	1.360×10^{-8}	6.120×10^{-9}	600	1.653×10^{-8}	2.534×10^{-9}
70	9.930×10^{-9}	4.091×10^{-9}	800	1.959×10^{-8}	2.864×10^{-9}
80	7.708×10^{-9}	2.905×10^{-9}	1000	2.155×10^{-8}	3.126×10^{-9}

Figure A-15. Electron emission from aluminum behind box wall due to monoenergetic photons incident at 1 cal/cm^2

44

RE-01443

PHOTON	ELECTRON YIELD RATIOS		PHOTON	ELECTRON YIELD RATIOS	
ENERGY (keV)	FORWARD/ REVERSE	HIGH-Z/ LOW-Z	ENERGY (keV)	FORWARD/ REVERSE	HIGH-Z/ LOW-Z
2	1.035	5.336	90	2.926	118.7
5	1.211	56.93	100	3.215	96.60
10	1.323	87.72	125	4.016	59.01
15	1.435	208.2	150	4.762	39.17
20	1.528	285.5	200	5.601	17.73
30	1.705	332.1	300	6.061	6.063
40	1.849	348.9	400	6.253	2.974
50	2.044	316.8	500	6.390	2.034
60	2.223	264.8	600	6.523	1.357
70	2.427	196.2	800	6.839	0.9004
80	2.653	127.7	1000	7.121	0.7286

Figure A-16. Electron emission ratios due to monoenergetic photons. The high-to-low-Z ratio is for forward emission from gold compared to carbon. The forward-to-reverse ratio is for aluminum.

45
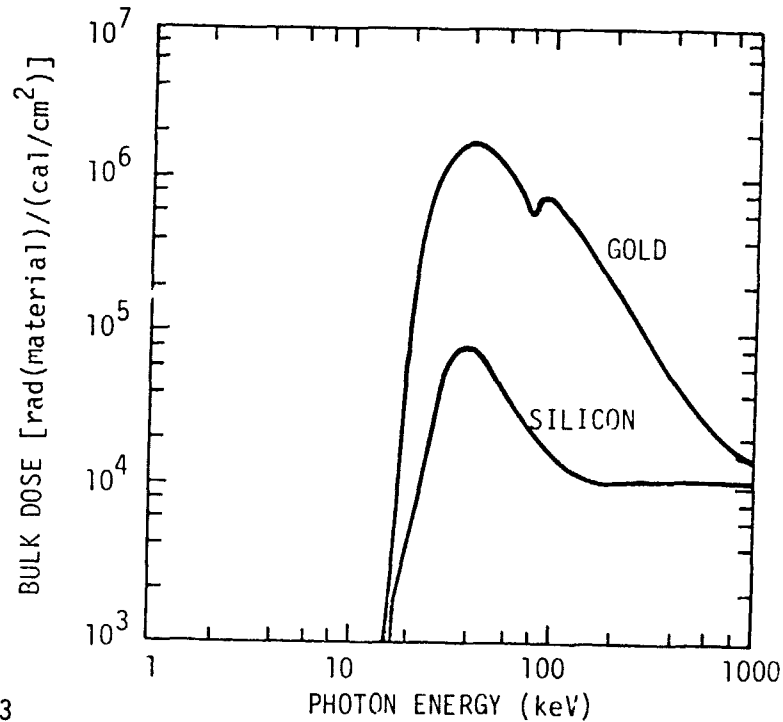
RE-01223

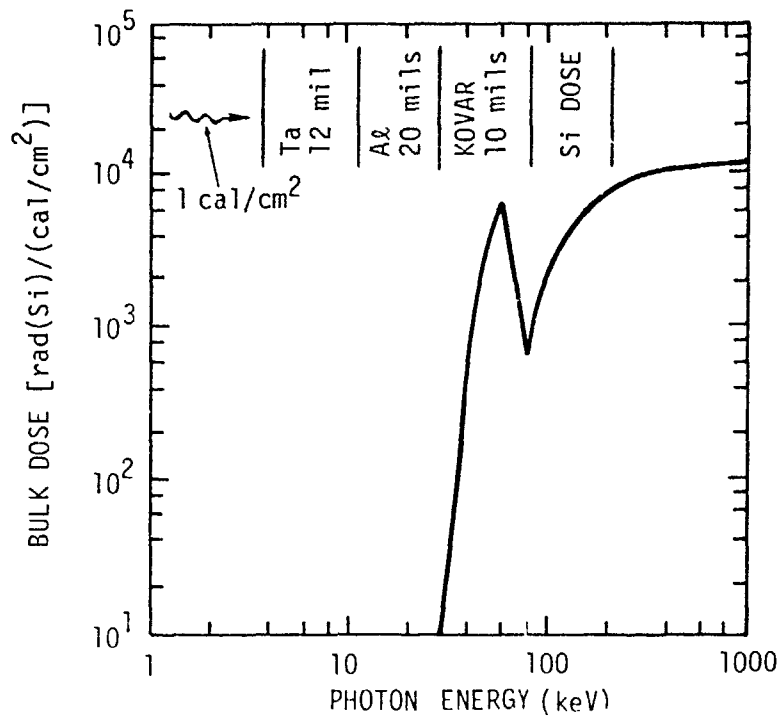| PHOTON ENERGY (keV)	BULK DOSE		PHOTON ENERGY (keV)	BULK DOSE	
	[rad(Au)]	[rad(Si)]		[rad(Au)]	[rad(Si)]
2	–	–	90	7.990×10^5	1.966×10^4
5	–	–	100	7.476×10^5	1.673×10^4
10	–	–	125	5.635×10^5	1.334×10^4
15	2.565×10^2	1.926×10^1	150	4.047×10^5	1.198×10^4
20	5.623×10^4	3.478×10^3	200	2.255×10^5	1.150×10^4
30	1.406×10^6	7.001×10^4	300	9.484×10^4	1.181×10^4
40	1.894×10^6	8.293×10^4	400	5.340×10^4	1.206×10^4
50	1.556×10^6	6.281×10^4	500	3.613×10^4	1.214×10^4
60	1.139×10^6	4.404×10^4	600	2.744×10^4	1.212×10^4
70	8.212×10^5	3.161×10^4	800	1.926×10^4	1.191×10^4
80	6.262×10^5	2.426×10^4	1000	1.555×10^4	1.160×10^4

Figure A-17. Bulk dose inside device housing due to monoenergetic photons incident at 1 cal/cm². The ratio of the two curves is shown in Figure A-13.

46

RE-01224

PHOTON ENERGY (keV)	BULK DOSE $[rad(Si)/cal/cm^2]$	PHOTON ENERGY (keV)	BULK DOSE $[rad(Si)/cal/cm^2]$
2	-	90	1.202×10^3
5	-	100	1.980×10^3
10	-	125	3.985×10^3
15	-	150	5.620×10^3
20	-	200	7.904×10^3
30	1.332×10^0	300	1.011×10^4
40	5.340×10^2	400	1.100×10^4
50	3.771×10^3	500	1.158×10^4
60	6.607×10^3	600	1.205×10^4
70	1.705×10^3	800	1.209×10^4
80	6.973×10^2	1000	1.169×10^4

Figure A-18. Dose inside shielded box due to monoenergetic photons incident at 1 cal/cm²

47

APPENDIX B

EXCITATION PARAMETER RESULTS
FOR BLACKBODY SPECTRA
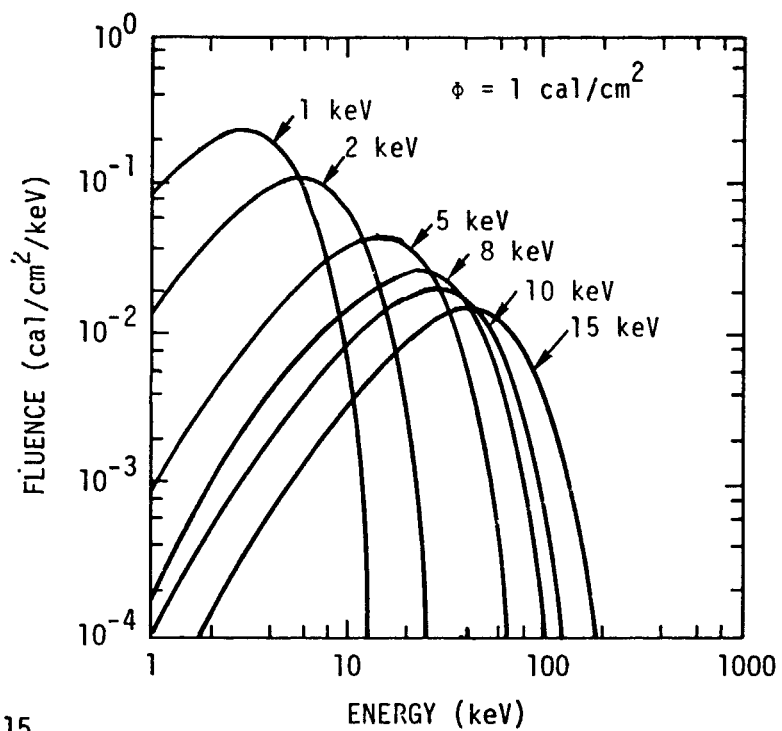
RE-01115

Figure B-1. Blackbody photon spectra

10^8

10^7

10^6

10^5

10^4

DOSE [rad(material)/(cal/cm^2)]

SURFACE
DOSE

DOSE   ●Si
AT   OR
INTERFACE   MYLAR

SILICON

MYLAR

0   10   20   30

BLACKBODY TEMPERATURE (keV)
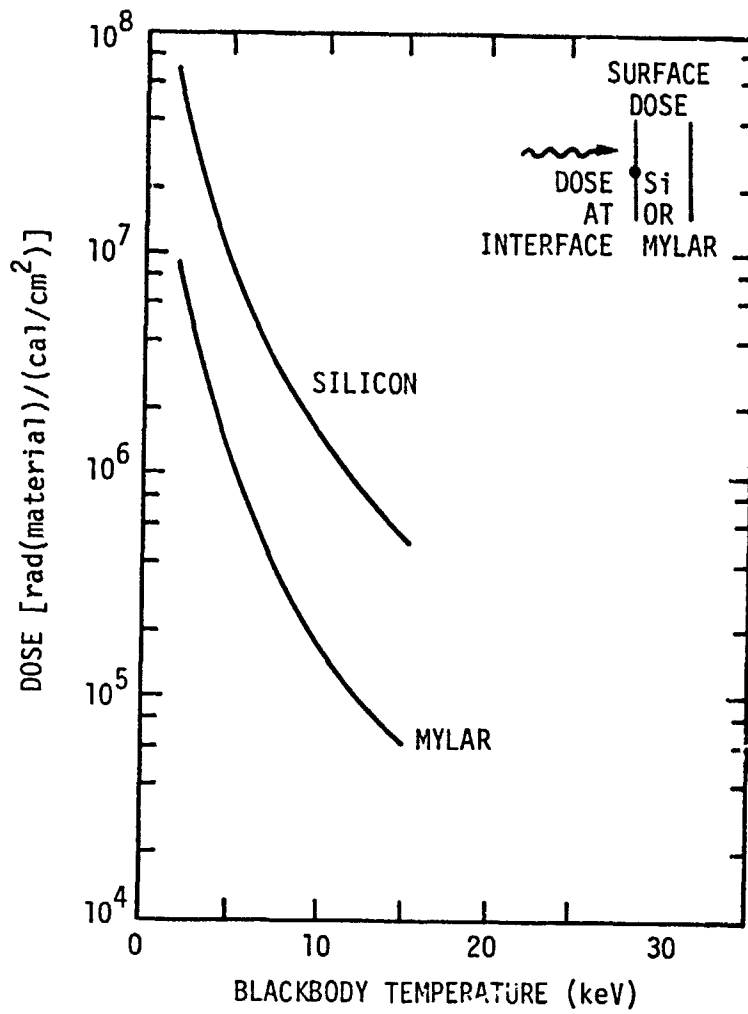
RE-01444

Figure B-2.   Interface dose at the surface of dielectric materials
due to blackbody photon spectra incident at 1 cal/cm^2
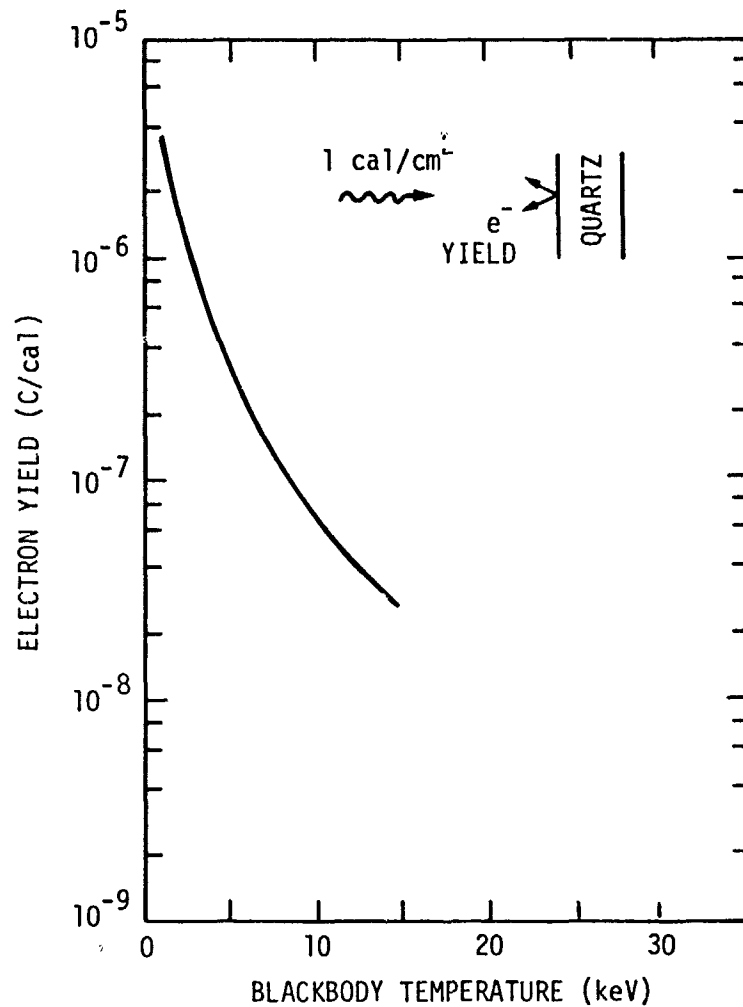
RE-01445

BLACKBODY TEMPERATURE (keV)	ELECTRON YIELD (C/cal)
1	3.41×10^{-6}
2	1.40×10^{-6}
5	2.86×10^{-7}
8	1.08×10^{-7}
10	6.60×10^{-8}
15	2.85×10^{-8}

Figure B-3. Electron yield at the surface of quartz due to black-body photon spectra incident at 1 cal/cm^2

52
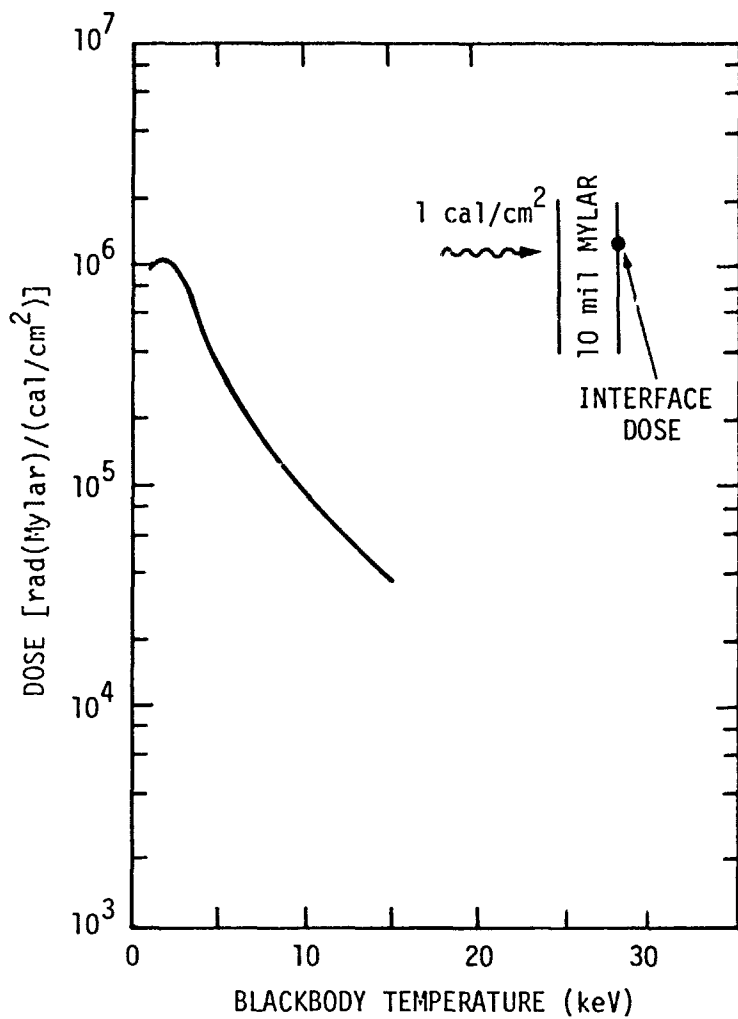
RE-01454

BLACKBODY TEMPERATURE (keV)	INTERFACE DOSE [rad(Mylar)]
1	1.03×10^6
2	1.10×10^6
5	3.42×10^5
8	1.42×10^5
10	8.80×10^4
15	3.80×10^4

Figure B-4. Interface dose behind thermal blanket due to blackbody photon spectra incident at 1 cal/cm^2

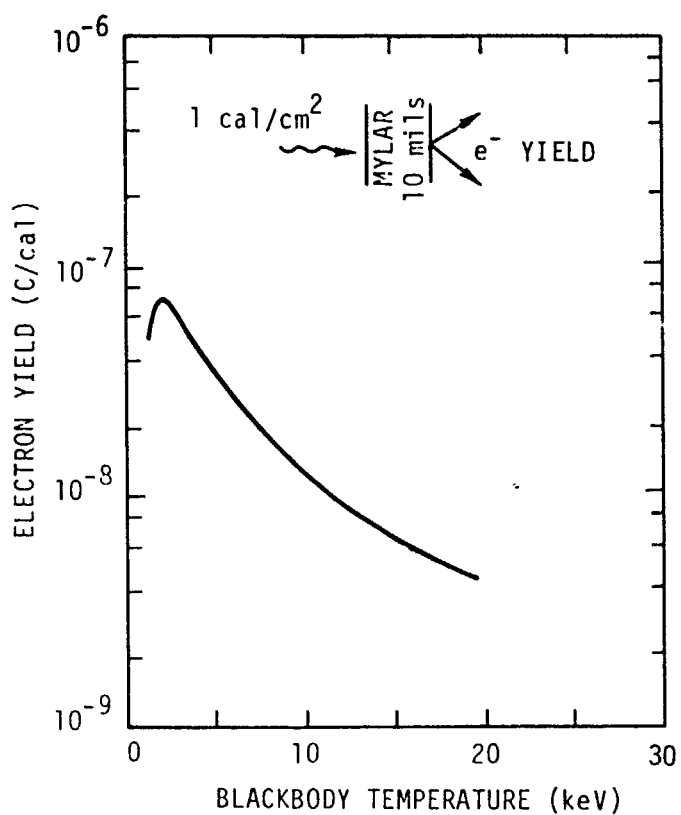| BLACKBODY TEMPERATURE (keV)	ELECTRON YIELD (C/cal)
1	5.99×10^{-8}
2	8.13×10^{-8}
5	3.56×10^{-8}
8	1.86×10^{-8}
10	1.30×10^{-8}
15	6.20×10^{-9}

Figure B-5. Electron yield behind thermal blanket due to black-
body photon spectra incident at 1 cal/cm^2
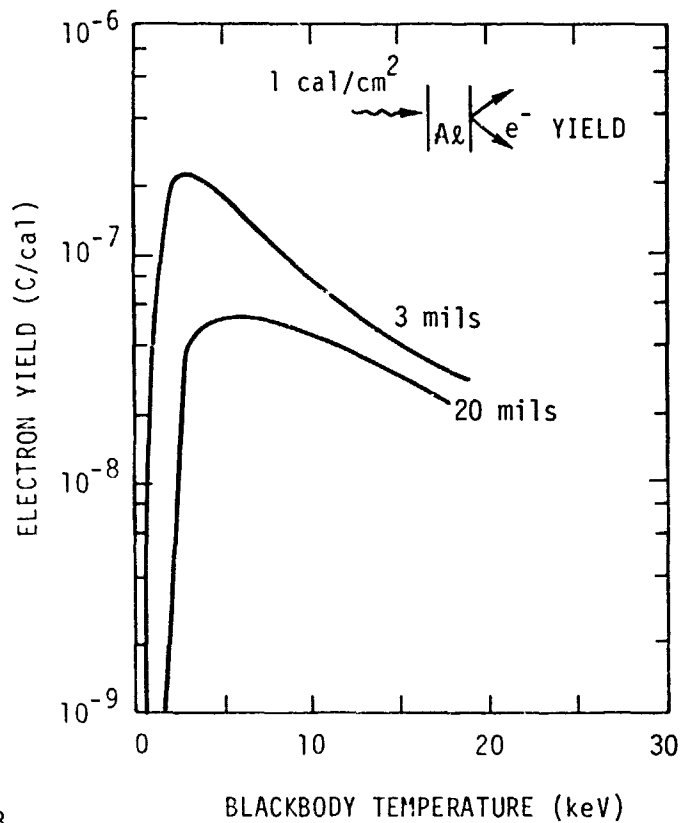
RE-01079B

BLACKBODY TEMPERATURE (keV)	ELECTRON YIELD (C/cal)	
	3 mils	20 mils
1	5.54×10^{-8}	4.85×10^{-10}
2	2.00×10^{-7}	1.65×10^{-8}
5	1.82×10^{-7}	5.92×10^{-8}
8	1.10×10^{-7}	5.23×10^{-8}
10	8.06×10^{-8}	4.41×10^{-8}
15	4.31×10^{-8}	2.76×10^{-8}

Figure B-6.   Electron yield forward-emitted from aluminum after penetration of 3 and 20 mils aluminum by blackbody photon spectra

55
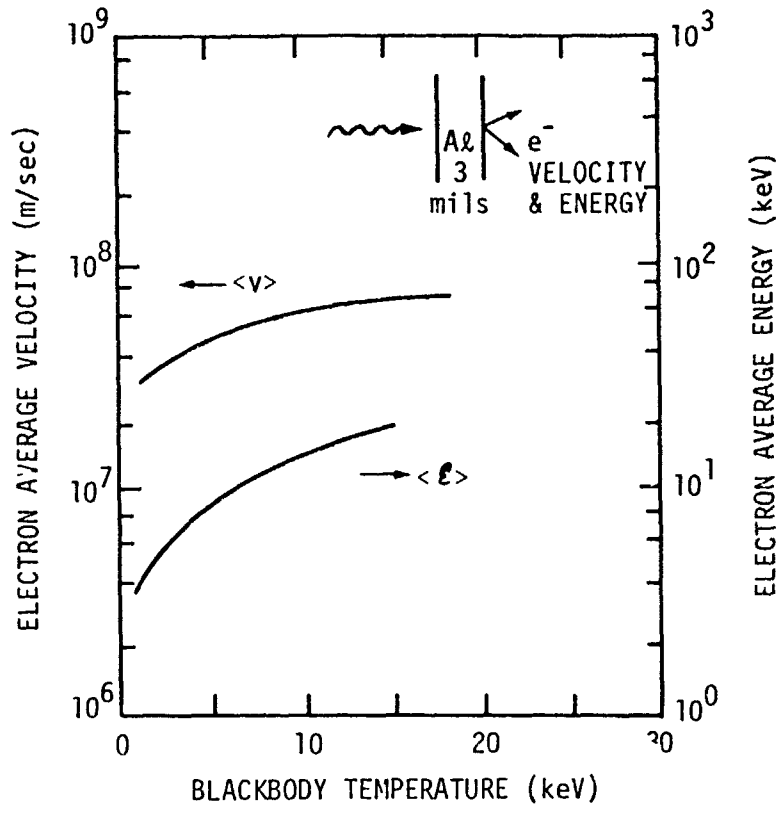
RE-01086B

BLACKBODY TEMPERATURE (keV)	AVERAGE ELECTRON VELOCITY (m/sec)	AVERAGE ELECTRON ENERGY (keV)
1	3.26×10^7	3.79
2	3.80×10^7	5.42
5	4.73×10^7	9.11
8	5.33×10^7	12.4
10	5.64×10^7	14.4
15	6.26×10^7	19.2

Figure B-7. Average velocity and energy of electrons emitted from 3 mils aluminum due to blackbody photon spectra incident

56
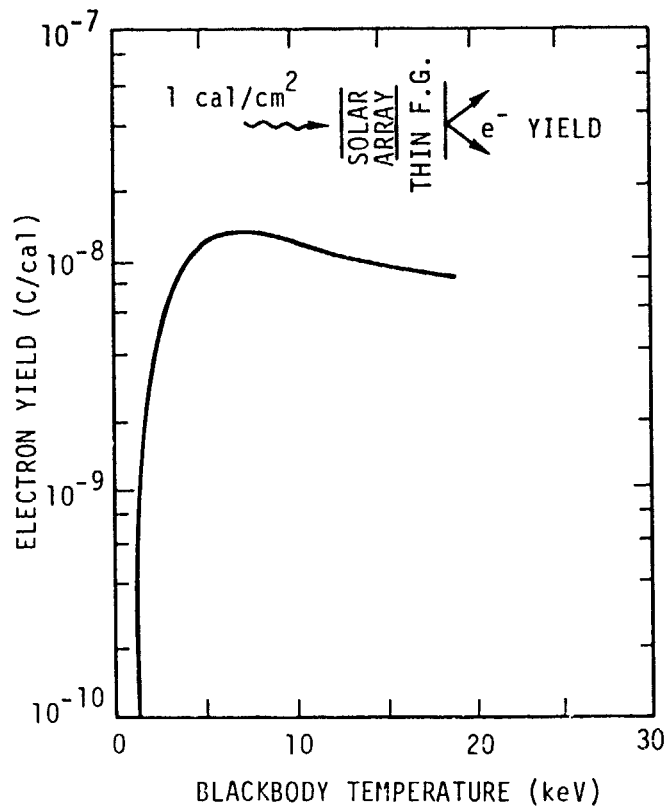
RE-00986B

BLACKBODY TEMPERATURE (keV)	ELECTRON YIELD (C/cal)
2	2.02×10^{-9}
5	1.28×10^{-8}
8	1.41×10^{-8}
10	1.30×10^{-8}
15	9.50×10^{-9}

Figure B-8. Electron yield behind solar array due to blackbody photon spectra incident at 1 cal/cm^2
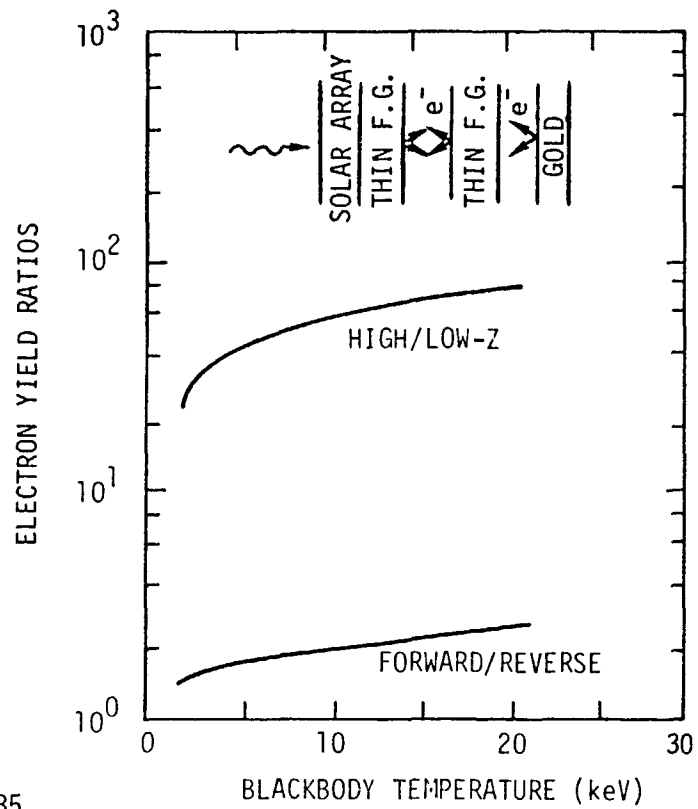
RE-01085

BLACKBODY TEMPERATURE (keV)	ELECTRON YIELD RATIOS	
	FORWARD/REVERSE	HIGH/LOW-Z
2	1.52	31.6
5	1.68	50.5
8	1.77	57.5
10	1.88	62.5
15	2.05	73.2

Figure B-9. Electron emission ratios behind solar array due to blackbody photon spectra incident

58
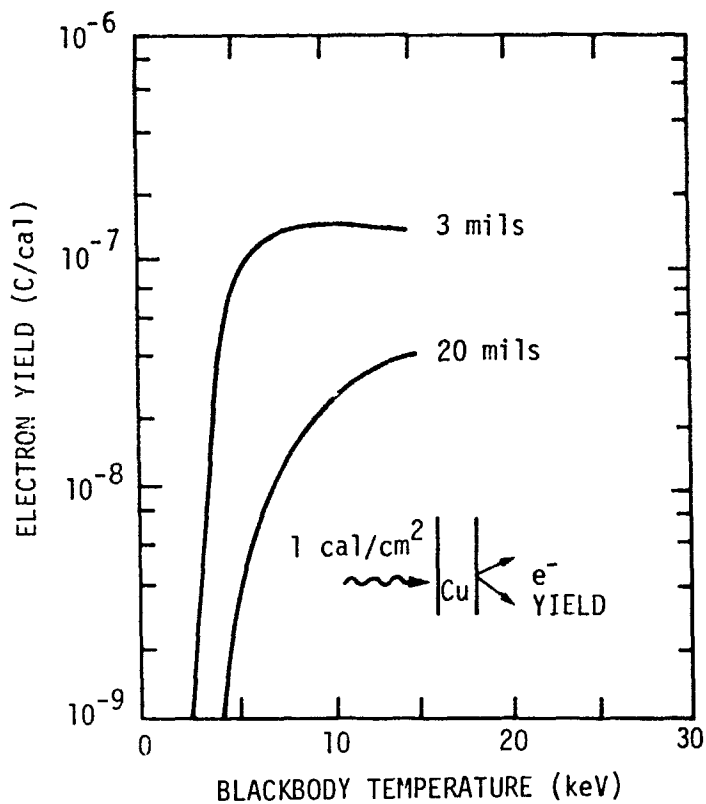
RE-01081B

BLACKBODY TEMPERATURE (keV)	ELECTRON YIELD (C/cal)	
	3 mils	20 mils
2	9.13×10^{-9}	5.70×10^{-13}
5	8.97×10^{-8}	3.93×10^{-9}
8	1.48×10^{-7}	1.83×10^{-8}
10	1.50×10^{-7}	2.77×10^{-8}
15	1.40×10^{-7}	4.09×10^{-8}

Figure B-10. Electron yield inside cables of shield thicknesses 3 and 20 mils due to blackbody photon spectra incident at 1 cal/cm^2
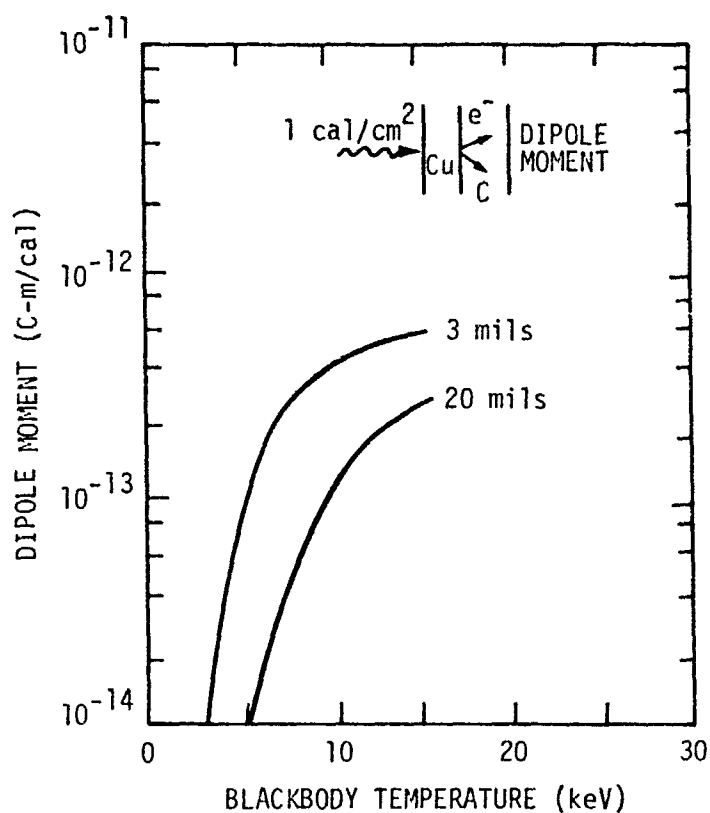
RE-01080A

BLACKBODY TEMPERATURE (keV)	DIPOLE MOMENT (C-m/cal)	
	3 mils	20 mils
2	1.96×10^{-15}	-
5	9.80×10^{-14}	9.98×10^{-15}
8	2.80×10^{-13}	7.25×10^{-14}
10	3.78×10^{-13}	1.36×10^{-13}
15	5.52×10^{-13}	2.97×10^{-13}

Figure B-11. Dipole moment inside cable dielectric due to blackbody photon spectra incident at 1 cal/cm^2. Copper shield thicknesses are indicated beside the curves.

60
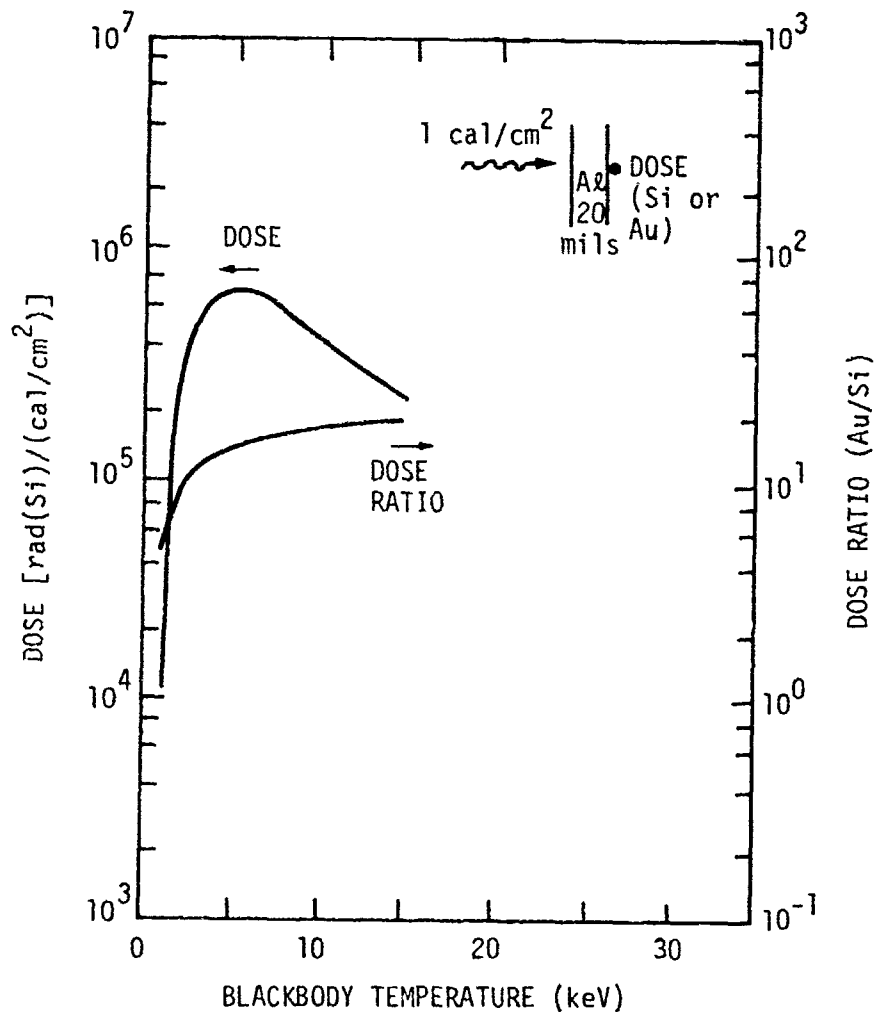
RE-01446

BLACKBODY TEMPERATURE (keV)	BULK DOSE [rad(Si)]	BULK DOSE RATIO (Au/Si)
1	1.15×10^4	4.84
2	2.88×10^5	9.43
5	7.39×10^5	14.0
8	5.50×10^5	15.7
10	4.21×10^5	16.7
15	2.29×10^5	18.4

Figure B-12. Bulk dose and dose ratio inside box due to blackbody photon spectra incident at 1 cal/cm²
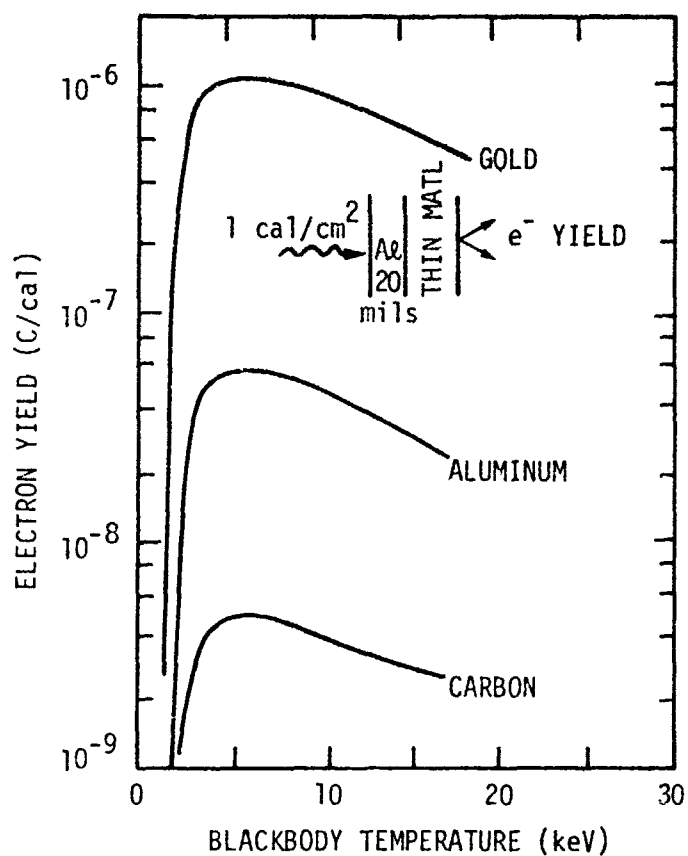
RE-01447

BLACKBODY TEMPERATURE (keV)	ELECTRON YIELD (C/cal)		
	Carbon	Aluminum	Gold
1	4.82×10^{-11}	4.85×10^{-10}	4.34×10^{-9}
2	1.40×10^{-9}	1.65×10^{-8}	2.12×10^{-7}
5	4.40×10^{-9}	5.92×10^{-8}	1.07×10^{-6}
8	3.81×10^{-9}	5.23×10^{-8}	1.04×10^{-6}
10	3.27×10^{-9}	4.41×10^{-8}	9.08×10^{-7}
15	2.56×10^{-9}	2.76×10^{-8}	6.31×10^{-7}

Figure B-13. Forward-emitted electron yield inside box due to blackbody photon spectra incident at 1 cal/cm^2
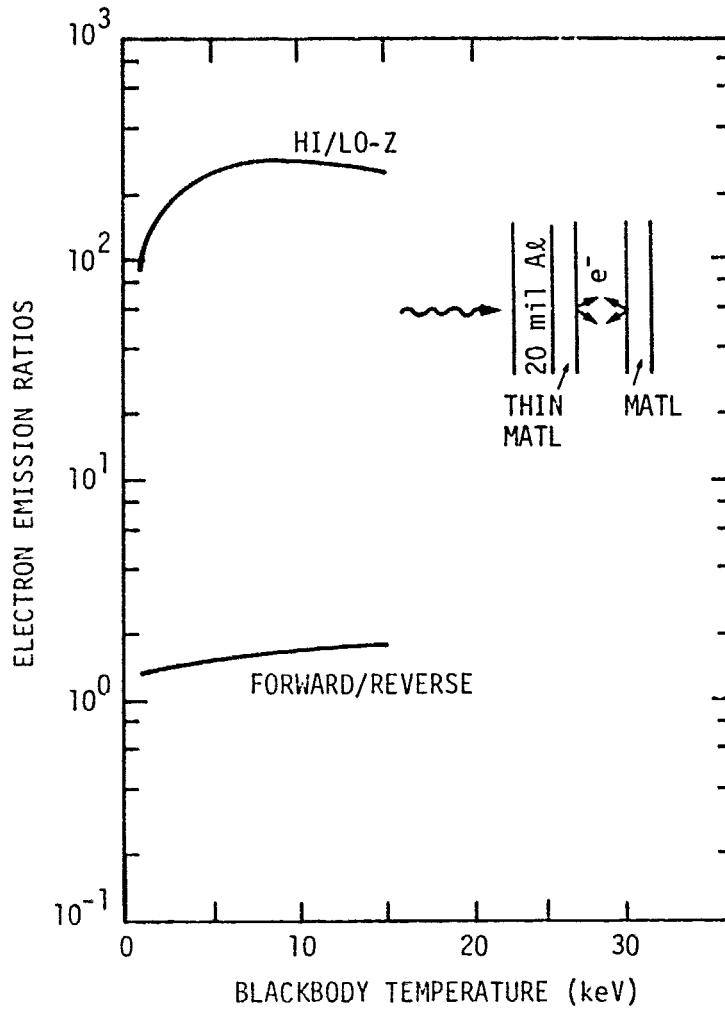
RE-01448

Figure B-14. Electron emisson ratios inside box due to blackbody
photon spectra. The high-to-low-Z emission ratio is
for forward emission from gold compared to carbon.
The forward-to-reverse ratio is for aluminum.
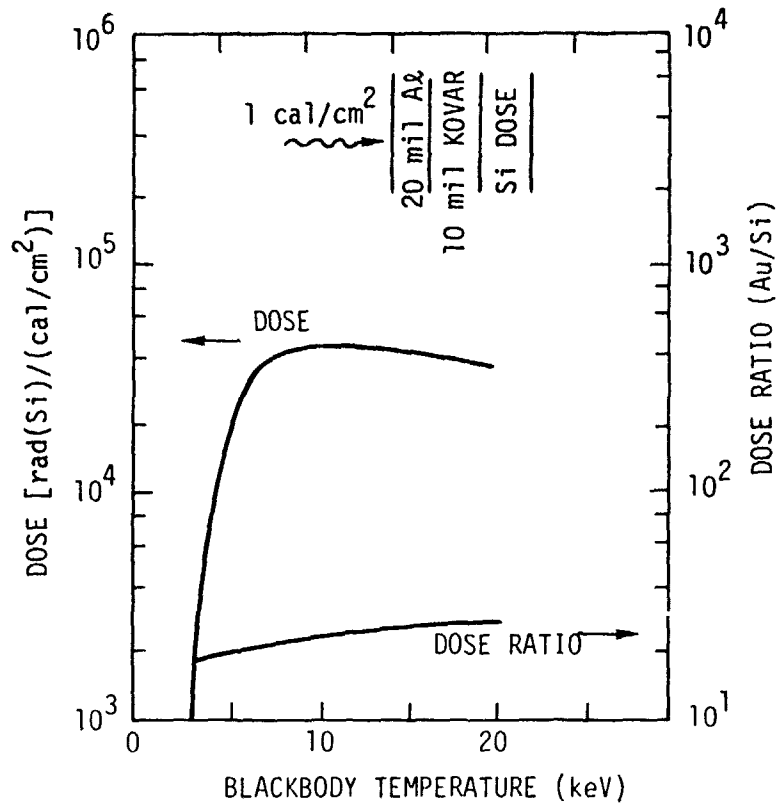
RE-01083

BLACKBODY TEMPERATURE (keV)	BULK DOSE [rad(Si)]	BULK DOSE RATIO (Au/Si)
5	1.84×10^4	20.6
8	3.95×10^4	21.8
10	4.53×10^4	22.7
15	4.31×10^4	24.6

Figure B-15. Bulk dose and dose ratio inside device housing due to blackbody photon spectra incident at 1 cal/cm^2

64
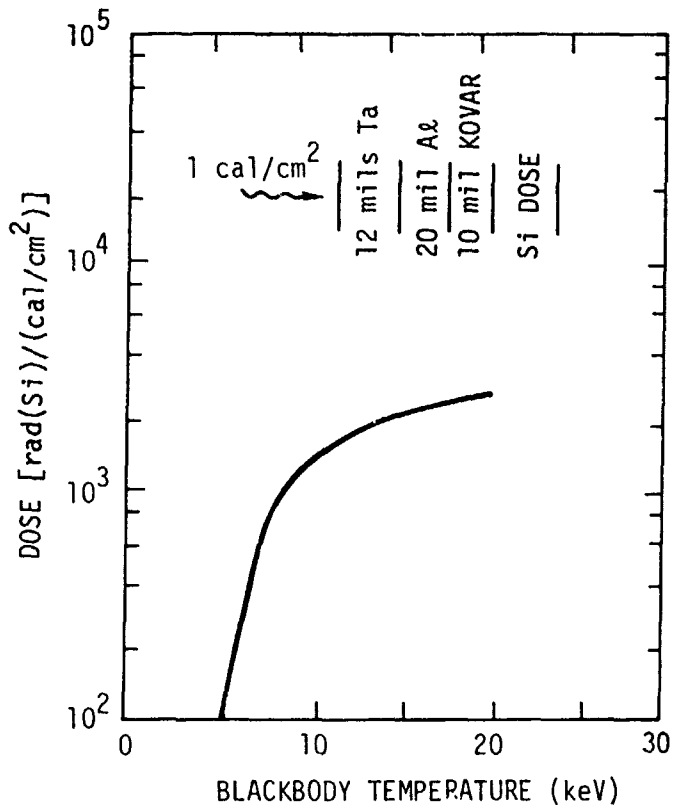
RE-01213

BLACKBODY TEMPERATURE (keV)	DOSE [rad(Si)]
5	1.34×10^2
8	8.93×10^2
10	1.41×10^3
15	2.19×10^3
20	2.69×10^3

Figure B-16.   Dose inside shielded box due to blackbody photon spectra incident at 1 cal/cm^2

APPENDIX C

RESPONSE PARAMETER RESULTS
FOR BLACKBODY SPECTRA
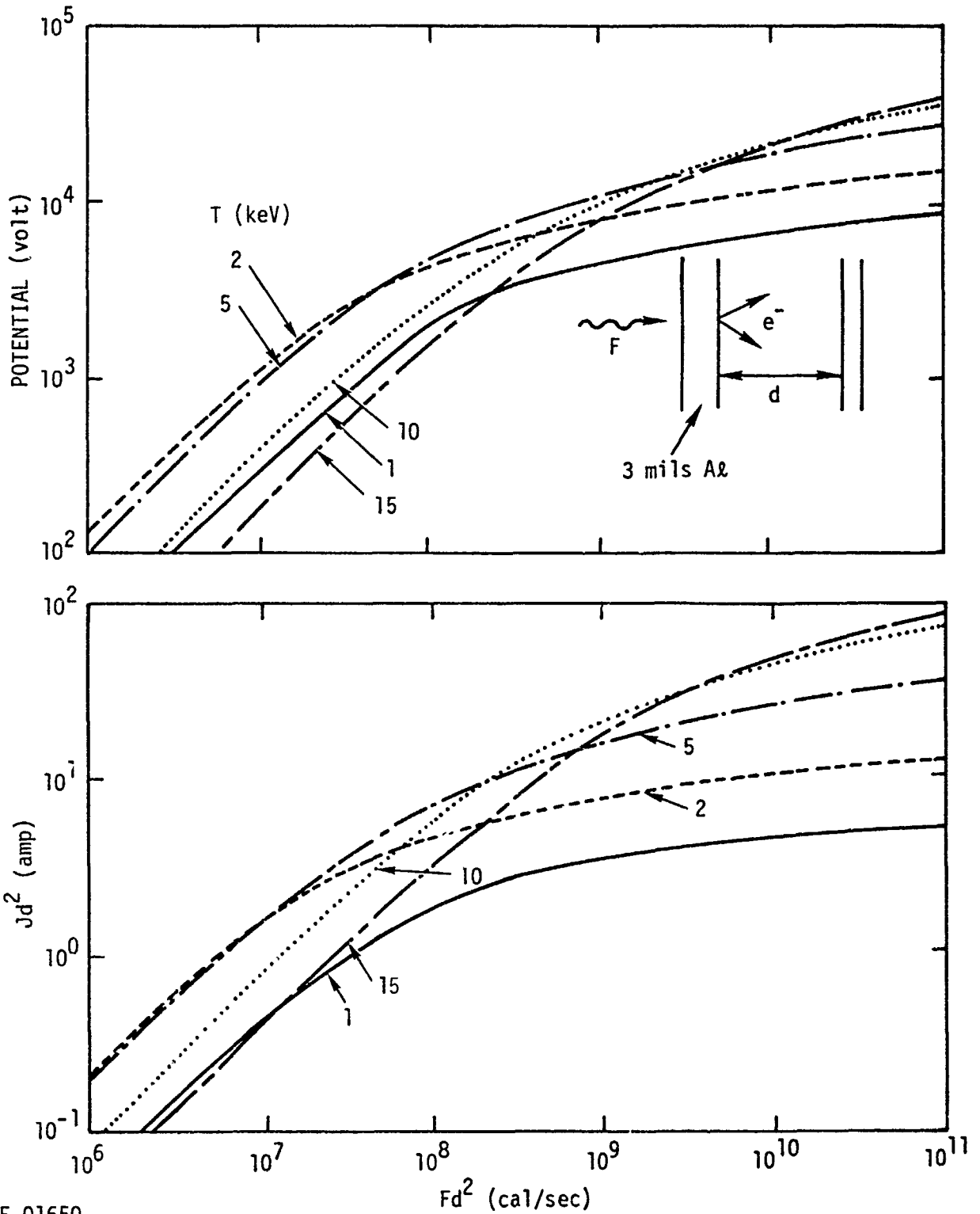
Figure C-1. Diode potential and scaled current due to incident blackbody spectra of temperature T (keV). F is the photon flux, J is the electron current density, and d is the plate spacing.
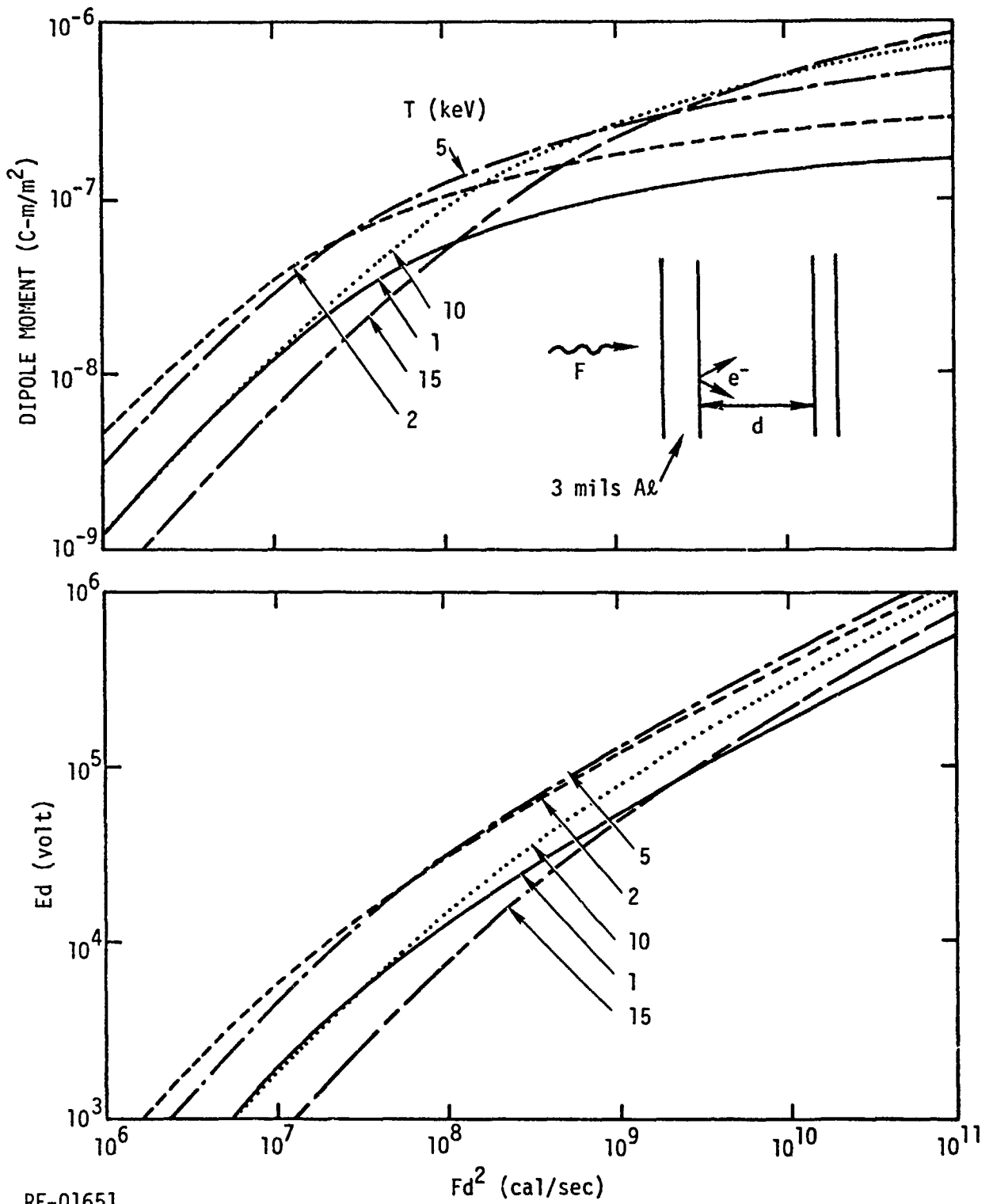
RE-01650

Figure C-2. Dipole moment and scaled electric field at the front face of a diode due to incident blackbody spectra of temperature T (keV). F is the photon flux, E is the electric field, and d is the plate spacing.

RE-01651

69
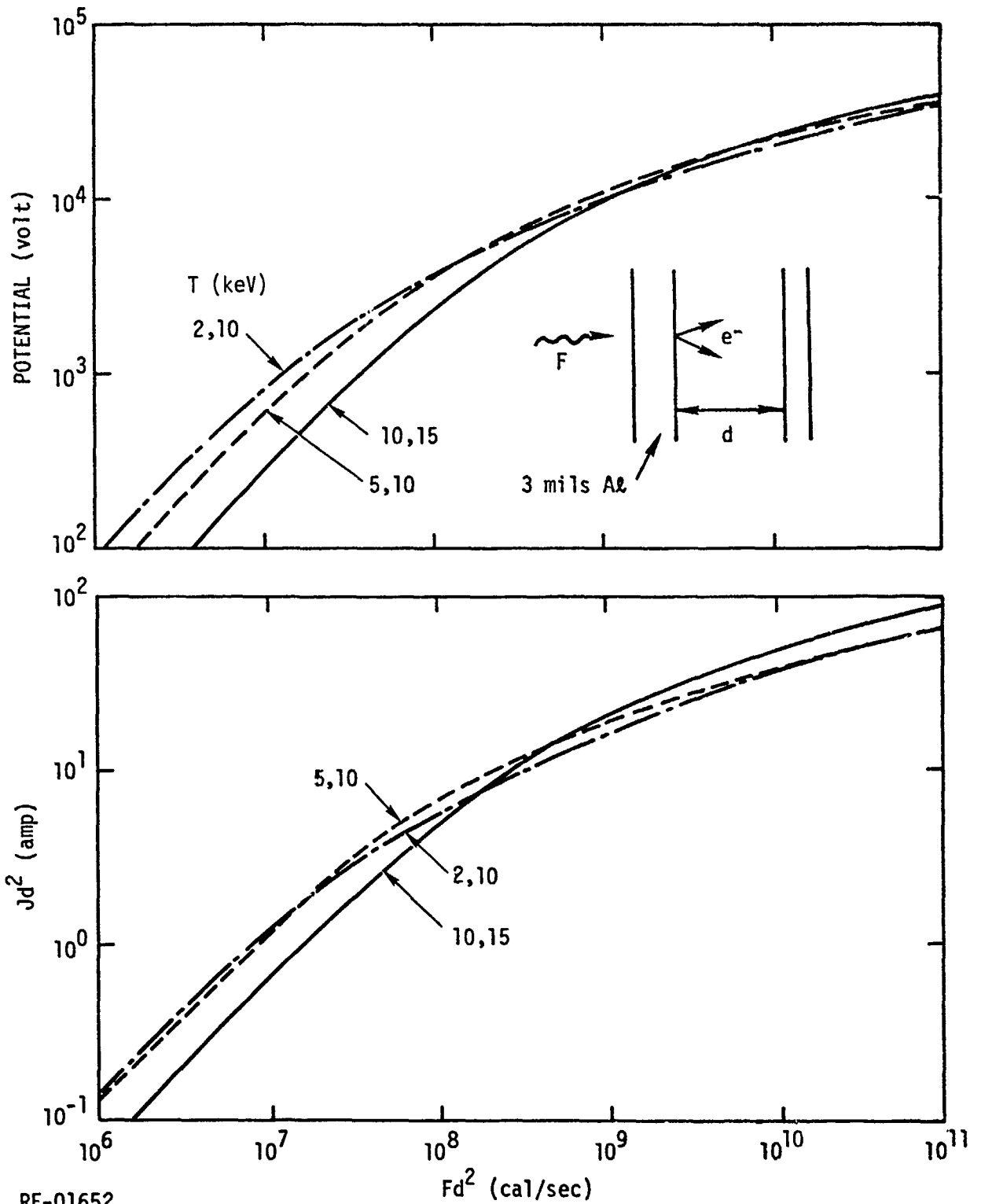
RE-01652

Figure C-3. Diode potential and scaled current due to blackbody combination spectra. Equal fluxes of temperature T (indicated in keV) are incident. F is the photon flux, J is the electron current, and d is the plate spacing.
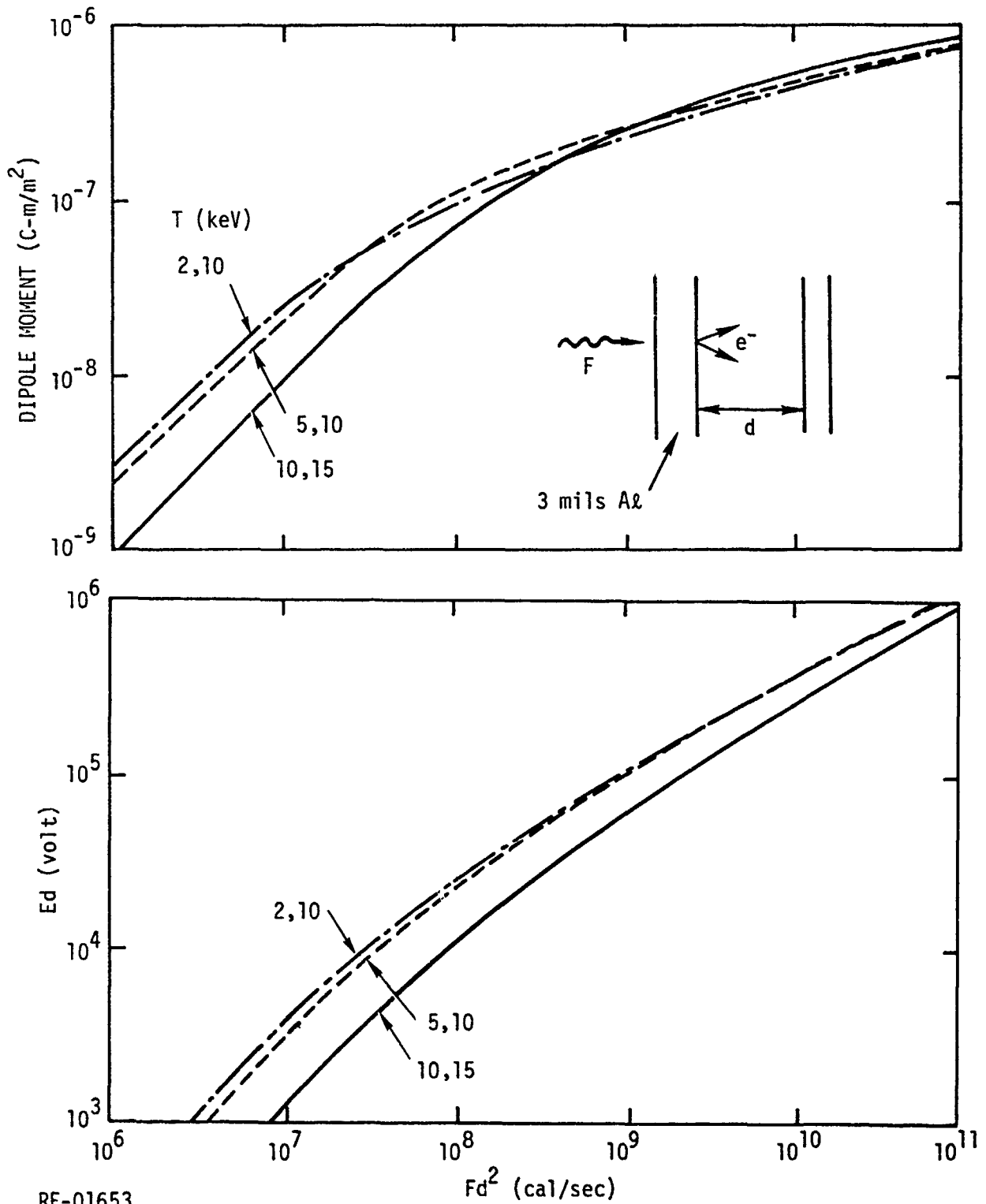
RE-01653

Figure C-4. Dipole moment and scaled electric field at the front face of a diode due to blackbody combination spectra. Equal fluxes of temperature T (indicated in keV) are incident. F is the photon flux, E is the electric field, and d is the plate spacing.

71

APPENDIX D

PROGRAMMABLE CALCULATOR CODES FOR
ARBITRARY SPECTRUM COMPUTATIONS

The excitation parameters discussed in Section 4 of this report are conveniently obtainable for arbitrary photon spectra by means of programmable calculator codes described here. The programs are designed for use on the Texas Instruments TI-59 calculator and are available on magnetic cards. Arbitrary spectra can be keyed in or read in from magnetic cards, and the calculator will automatically compute the excitation parameters. Brief descriptions of the codes and specific user instructions follow.

D.1 CODE OVERVIEW

A brief overview of the codes is helpful in understanding their operation. The calculator memory is divided into four banks which can be programmed with up to 240 steps each. Memory can be partitioned to interchange code steps and data storage, with up to 30 numbers stored in each bank. One insertion of a magnetic card sets all locations in a bank of memory. Therefore, the memory has been programmed according to the divisions shown in Table D-1. The memory allocation shown limits the program to only 240 steps, but it has the considerable advantage of permitting spectra to be stored on one set of cards and excitation parameter data on another set. The user may read in a spectrum to bank 2 and compute parameters for different satellite configurations by simply reading in different data to bank 3 and repeating the calculation.

Table D-1. TI-59 Memory Allocation for Computation of
           Spectrum Evaluation Parameters

Bank 1	Program	Up to 240 steps
Bank 2	Spectrum	Up to 14 point pairs
Bank 3	Excitation parameter curves	Up to 15 point pairs
Bank 4	Working storage	

D.2 USER INSTRUCTIONS

Step-by-step instructions for using the programs are given below. The user is assumed to have an elementary knowledge of the calculator.

74

D.2.1 Setup

Partition calculator memory to 240 maximum program steps with 90 data locations:

- Press 9 Op 17
- Press CLR
- Insert program card (called ARBSPC)

Calculator will display 1, indicating bank 1 has been programmed.

D.2.2 Spectrum Input

- Punch spectrum into memory bank 2:

Energies (keV)	locations 60-73
Differential fluence (energy/energy/area)	locations 75-88

  (To save this spectrum on a card, press CLR, then WRITE, and insert a blank card.)

Up to 14 energies and 14 differential fluences may be input. A spectrum may be read in from a card by pressing CLR and inserting the card. The calculator will display 2., indicating memory bank 2 has been programmed. See optional input routine, TLBSET, for rapid spectrum input. Spectra are normalized automatically by the code. Photon energies must be less than 1000 keV. Spectra must have at least three energy bins.

D.2.3 Excitation Parameter Data Input

Read selected excitation parameter weighting factor (see Appendix A) into locations 30-59 (bank 3):

- Press CLR
- Insert card

Calculator displays 3., indicating bank 3 has been programmed.

D.2.4 Execution

The calculator is now ready to compute the selected parameter for the spectrum chosen.

- Press RST
- Press R/S

Execution commences and numbers flash on the display for each energy bin in the order below.

ϵ_i ith bin energy (keV)

$\Phi_{0\epsilon_i}$ ith differential fluence (energy/energy/area)

$\sum_i \Phi_{0\epsilon_i} \Delta\epsilon_i$ cumulative sum of fluences in each bin (energy/area)

When the display becomes fixed, the value is total fluence:

$$\sum_{i=1}^{Nbins} \Phi_{0\epsilon_i} \Delta\epsilon_i \quad \text{(energy/area)}$$

where Nbins is the total number of energy bins. This is the total fluence incident on the exterior of the excitation parameter configuration chosen.

         Press <u>R/S</u>

Calculator displays Excitation Parameter P (per unit fluence).

         Press <u>R/S</u>

Calculator displays ratio $P_{previous}/P_{current}$, the ratio of the previously calculated excitation parameter to the current one. Thus, if a dose ratio Au/Si is being computed, for example, the dose for gold is computed first, then a new card read in for silicon and the process repeated. The third static display yields the ratio on the second pass.

         The execution steps are summarized in Table D-2.

D.2.5   Optional Spectrum Input Routine

         A routine is available to expedite table entries and checkouts. In our case, we want to input a string of energies into memory beginning at location 60, and the corresponding differential fluences beginning at location 75.

         To perform this operation, press <u>9 Op 17</u> to partition memory, then read in the TLBSET code card. Press <u>RST</u>, then <u>R/S</u>. The calculator now displays 1., indicating energy bin 1. Energies may now be input by keying them in and pressing <u>R/S</u>. The index of the next bin then appears. To indicate the last bin, enter a zero and the calculator will automatically

Table D-2. Summary of Program Setup and Execution, ARBSPC

Partition calculator: Press 9 Op 17

Input program   Bank 1

Input spectrum   Bank 2

Input data table   Bank 3

Press RST

Press R/S

Calculator pauses briefly for each energy bin and displays:

$$\epsilon_i$$

$$\Phi_{0\epsilon_i}$$

$$\sum_i \Phi_{0\epsilon_i} \Delta\epsilon_i$$

Calculator stops and displays:

$$\sum_{i=1}^{Nbins} \Phi_{0\epsilon_i} \Delta\epsilon_i \quad \text{(total fluence incident)}$$

    Press R/S. Calculator displays P (excitation parameter/cal/cm^2)

    Press R/S. Calculator displays ratio $P_{previous}/P_{current}$

To continue,

    Press CLR

    Read in new spectrum or data table

    Press RST

    Press R/S

---

skip to location 75 and display 1. for bin 1. At this point, begin entering differential fluences.

The values may be displayed in succession by pressing E and then R/S, R/S, etc. Displays beginning at any location can be commenced by entering the desired location and pressing A´. The calculator will automatically begin displaying at location 60 if no entry is made into A´.

A summary of TLBSET operations is given in Table D-3. A summary of calculator outputs is given in Table D-4.

Table D-3. Summary of Input/Output Routine TLBSET Instructions

Labels:	A´ Starting location for display (default = value in B)	B´	C´ Starting location to multiply, R/S, multiply by, R/S	D´	E´
		B Starting location for storage (default=60)	C	D	E Display values beginning at A´

- Press 9 Op 17
- Read in program TLBSET
- Press RST, R/S
- Enter beginning storage location in B (default value = 60)
- Enter energy, press R/S, energy, R/S, etc.
- Terminate string with 0., R/S
- Enter differential fluence, press R/S, etc.
- To display values, press E, R/S, R/S, . . .

  To display values beginning at a location other than B, enter the location in A´ after RST, then press E, R/S, R/S, . . .

Table D-4. Spectrum Evaluation Program Symbols and Units

Energy	ε	keV
Photon fluence	Φ	cal/cm^2
Photon differential fluence	Φ_ε	$cal/cm^2/keV$
Dose	D	rad(material)
Electron yield	Y	C/cal
Velocity	v	m/sec
Electron dipole moment	P	C-m/cal

DISTRIBUTION LIST

DEPARTMENT OF DEFENSE

Assistant to the Secretary of Defense
Atomic Energy
        ATTN: Executive Assistant

Defense Intelligence Agency
        ATTN: DB-4C

Defense Nuclear Agency
 2 cy ATTN: RAEV
 4 cy ATTN: TITL

Defense Technical Information Center
12 cy ATTN: DD

Field Command
Defense Nuclear Agency
        ATTN: FCLMC
        ATTN: FCPR

Field Command
Defense Nuclear Agency
Livermore Division
        ATTN: FCPRL

Interservice Nuclear Weapons School
        ATTN: TTV

Joint Chiefs of Staff
        ATTN: C3S, Evaluation Office
        ATTN: J-5, Nuclear Division

Joint Strat Tgt Planning Staff
        ATTN: JLA
        ATTN: JLTW-2

National Communications System
        ATTN: NCS-TS

Undersecretary of Def for Rsch & Engrg
        ATTN: Strategic & Space Systems (OS)
        ATTN: AE

DEPARTMENT OF THE ARMY

BMD Advanced Technology Center
Department of the Army
        ATTN: ATC-O

BMD Systems Command
Department of the Army
        ATTN: BDMSC-H

Deputy Chief of Staff for Rsch Dev & Acq
Department of the Army
        ATTN: DAMA-CSS-N

Electronics Tech & Devices Lab
U.S. Army Electronics R & D Command
        ATTN: DRSEL

DEPARTMENT OF THE ARMY (Continued)

Harry Diamond Laboraatories
Department of the Army
        ATTN: DELHD-N-RBC, R. Gilbert
        ATTN: DELHD-I-TL

U.S. Army Communications Sys Agency
        ATTN: CCM-AD-LB

U.S. Army Foreign Science & Tech Ctr
        ATTN: DRXST-IS-1

U.S. Army Missile Command
        ATTN: RSIC

DEPARTMENT OF THE NAVY

Naval Research Laboratory
        ATTN: Code 6707, K. Whitney
        ATTN: Code 7550, J. Davis
        ATTN: Code 6701

Naval Surface Weapons Center
        ATTN: Code F31

Strategic Systems Project Office
Department of the Navy
        ATTN: NSP

DEPARTMENT OF THE AIR FORCE

Air Force Geophysics Laboratory
        ATTN: PH, C. Pike

Air Force Weapons Laboratory
Air Force Systems Command
        ATTN: SUL
        ATTN: NT
        ATTN: NXS
 2 cy ATTN: DYC

Ballistic Missile Office
Air Force Systems Command
        ATTN: MNNH
        ATTN: MNRTE
        ATTN: MNNG

Research Development & Acq
Department of the Air Force
        ATTN: AFRDQSM

Headquarters Space Division
Air Force Systems Command
        ATTN: SKF

Rome Air Development Center
Air Force Systems Command
        ATTN: ESR, E. Burke

Strategic Air Command
Department of the Air Force
        ATTN: NRI-STINFO Library
        ATTN: XPFS

OTHER GOVERNMENT AGENCIES

Central Intelligence Agency
    ATTN: OSWR/STD/MTB, A. Padgett

NASA
Lewis Research Center
    ATTN: N. Stevens
    ATTN: C. Purvis
    ATTN: Library

DEPARTMENT OF ENERGY CONTRACTORS

Lawrence Livermore National Laboratory
    ATTN: Technical Information Dept Library

Los Alamos National Scientific Laboratory
    ATTN: MS 364

Sandia National Laboratories
Livermore Laboratory
    ATTN: T. Dellin

Sandia National Laboratories
    ATTN: Mail Services Section for 3141

DEPARTMENT OF DEFENSE CONTRACTORS

Aerospace Corp.
    ATTN: Library
    ATTN: V. Jcephson

AVCO Research & Systems Group
    ATTN: Library A830

Boeing Co.
    ATTN: P. Geren

Computer Sciences Corp.
    ATTN: A. Schiff

Dikewood Industries, Inc.
    ATTN: Technical Library

Dikewood Industries, Inc.
    ATTN: K. Lee

EG&G Washington Analytical Services Center, Inc.
    ATTN: Library

Ford Aerospace & Communications Corp.
    ATTN: Technical Library
    ATTN: A. Lewis

General Electric Co.
    ATTN: J. Peden

General Electric Company-TEMPO
    ATTN: W. McNamara
    ATTN: DASIAC

Hughes Aircraft Co.
    ATTN: Technical Library

Hughes Aircraft Co.
    ATTN: E. Smith
    ATTN: W. Scott
    ATTN: A. Narevsky

DEPARTMENT OF DEFENSE CONTRACTORS (Continued)

Institute for Defense Analyses
    ATTN: Classified Library

IRT Corp.
    ATTN: Library
    ATTN: N. Rudie

JAYCOR
    ATTN: Library
    ATTN: E. Wenaas

JAYCOR
    ATTN: R. Sullivan

Johns Hopkins University
    ATTN: P. Partridge

Kaman Sciences Corp.
    ATTN: Library
    ATTN: W. Rich
    ATTN: D. Osborn

Lockheed Missiles & Space Co., Inc
    ATTN: Dept 85-85

McDonnell Douglas Corp.
    ATTN: S. Schneider

Mission Research Corp.
    ATTN: C. Longmire
    ATTN: R. Stettner

Mission Research Corp.
    ATTN: B. Goplen

Mission Research Corp.
    ATTN: Library
    ATTN: V. Van Lint

R & D Associates
    ATTN: Technical Information Center
    ATTN: S. Siegel
    ATTN: P. Haas
    ATTN: T. Schaeffer

Rockwell International Corp.
    ATTN: Library

Science Applications, Inc.
    ATTN: W. Chadsey

Spire Corp.
    ATTN: R. Little

SRI International
    ATTN: Library

Systems Science & Software, Inc.
    ATTN: A. Wilson
    ATTN: Library

TRW Defense & Space Sys Group
    ATTN: Technical Information Center
    ATTN: D. Clement

82